Journal of Elasticity **61:** 1–48, 2000.

A New Constitutive Framework for Arterial Wall Mechanics and a Comparative Study of Material Models

GERHARD A. HOLZAPFEL and THOMAS C. GASSER
Institute for Structural Analysis – Computational Biomechanics, Graz University of Technology, 8010 Graz, Schiesstattgasse 14-B, Austria

RAY W. OGDEN
Department of Mathematics, University of Glasgow, University Gardens, Glasgow G12 8QW, U.K.

Received 20 April 2000; in revised form 8 December 2000

Abstract. In this paper we develop a new constitutive law for the description of the (passive) mechanical response of arterial tissue. The artery is modeled as a thick-walled nonlinearly elastic circular cylindrical tube consisting of two layers corresponding to the media and adventitia (the solid mechanically relevant layers in healthy tissue). Each layer is treated as a fiber-reinforced material with the fibers corresponding to the collagenous component of the material and symmetrically disposed with respect to the cylinder axis. The resulting constitutive law is orthotropic in each layer. Fiber orientations obtained from a statistical analysis of histological sections from each arterial layer are used. A specific form of the law, which requires only *three* material parameters for each layer, is used to study the response of an artery under combined axial extension, inflation and torsion. The characteristic and very important residual stress in an artery *in vitro* is accounted for by assuming that the natural (unstressed and unstrained) configuration of the material corresponds to an open sector of a tube, which is then closed by an initial bending to form a load-free, but stressed, circular cylindrical configuration prior to application of the extension, inflation and torsion. The effect of residual stress on the stress distribution through the deformed arterial wall in the physiological state is examined.

The model is fitted to available data on arteries and its predictions are assessed for the considered combined loadings. It is explained how the new model is designed to avoid certain mechanical, mathematical and computational deficiencies evident in currently available phenomenological models. A critical review of these models is provided by way of background to the development of the new model.

Mathematics Subject Classifications (2000): 74B20, 74E10, 74L15, 92C10.

Key words: biomechanics, arteries, artery wall, material models, constitutive laws, finite deformations, nonlinear elasticity.

1. Introduction

In the last few years there has been a significant growth in interest in the mechanical properties of biological soft tissue treated from the continuum mechanical perspective, and, in particular, in the mechanics of arterial tissue. An excellent starting point for the study of the mechanics of arteries is the wide-ranging review

by Humphrey [32], who, more recently [33], has conducted a comparative study of a small number of constitutive models used in the literature to describe the mechanical response of arteries. One important motivation for such studies is the belief that mechanical factors may be important in triggering the onset of atherosclerosis, the major cause of human mortality in the western world. In order to fully understand these mechanical influences it is necessary to have reliable constitutive models for the artery. Moreover, several clinical treatments, such as percutaneous transluminal angioplasty [3] can only be studied in detail if a reliable constitutive model of the arterial wall is available.

In vivo the artery is a pre-stretched material under an internal pressure load and it is essential to use a theory which takes account of the resulting finite deformation. The aim of this paper is therefore to provide a systematic study of the mechanical properties of arteries based on the continuum theory of large deformation elasticity. We begin, in Section 2, by giving a brief description of the histological structure of arterial walls, a summary of the main deformation geometries used in the experimental determination of the mechanical properties of arteries and an outline of the general characteristics of the mechanical response of arteries. It is emphasized that the vast majority of constitutive models used in the literature are phenomenological in nature and do not take account directly of the histological structure.

In Section 3 we summarize the theoretical framework to be used as the background for the description of the arterial mechanics. This consists of the general equations governing the elastic response of an *anisotropic* material based on the use of an elastic free-energy function. The equations are then specialized in order to consider the circular cylindrical geometry appropriate for the analysis of extension, inflation and torsion of an artery, which is treated as a thick-walled circular cylinder. In the absence of the applied loading, it should be emphasized, an artery is not stress free since if cut along a radius it will spring open to form an open sector. In this paper, for simplicity and in order to produce a distribution of residual stress in the unloaded configuration, we assume that the opened-up configuration is unstressed, although it is known that in general such a configuration is not unstressed (see, for example, Vossoughi et al. [64]). In general, there may also be residual stresses in the axial direction, but we do not allow for these in the present work. The assumed stress-free configuration is taken to correspond to an open sector of a circular cylindrical tube and is designated as the reference configuration of the material. The stressed but unloaded circular cylindrical shape is recovered by application of an initial bending deformation. Thus, the overall deformation from the reference configuration consists of bending, axial extension, inflation and torsion. This provides a composite deformation of sufficient generality to allow a comparative judgement of the predictions of different material models to be made.

In Section 4 a range of both two- and three-dimensional phenomenological models adopted in the literature for the study of *elastic* arteries is examined on the basis of the theory in Section 3 from a comparative point of view. Their performance is assessed critically against a number of criteria, and certain deficiencies

of the models are highlighted. Some anisotropic models are able to provide a full three-dimensional description of the state of stress in an artery, but at the expense of incorporation of a large number of material constants, which may lead to parameter identification problems. On the other hand, oversimplification through use of isotropy, as in Delfino et al. [10], is also evident. Several models, including that in Fung et al. [18], are based on formulations which may be associated with geometrical simplifications (for example, the membrane approximation) and are not suitable for analysis of the through-thickness stress distribution in an artery or for the treatment of shearing deformations. They can, however, be used to *simulate* the deformation in special cases, such as that corresponding to axial extension and inflation of an artery regarded as a thin-walled (or thick-walled) circular cylindrical tube. An approach which uses the incremental elastic moduli is also found in the literature (for some examples see the data book [1] edited by Abé et al.) but is not discussed here since it is inappropriate for the finite deformation analysis with which we are concerned.

One problem which arises in making comparisons is that each different model in the literature is based on data from a different artery (and generally from different animals). Nevertheless, we carry out a systematic and detailed evaluation of several of the most commonly used models in respect of combined extension, inflation and torsion of a thick-walled tube and with residual stresses incorporated. Moreover, a certain convexity property is introduced and checked for each model to provide an indication of its mechanical, mathematical and computational efficacy.

This provides the background for the introduction, in Section 5, of a new model which aims to circumvent the difficulties encountered with some other models. Specifically, the new model takes account of the architecture of the arterial wall. The artery is treated as a two-layer thick-walled tube, the two layers representing the media (the middle layer of the artery) and the adventitia (the outer layer). These are the main (solid) mechanically relevant components in healthy arteries. Thus, a third layer (the intima) is disregarded in this work, although it is not difficult to account for this on a similar basis as for the other layers if the need arises, which would be the case for arteries subject to pathological intimal change.

Each layer is composed of a non-collagenous matrix, which is treated as an isotropic material, and two families of collagen fibers helically wound along the arterial axis and symmetrically disposed with respect to the axis (but with different orientations in the two layers). These fibers induce the anisotropy in the mechanical response such that the overall response of each layer is orthotropic and is accounted for by the constitutive theory of fiber-reinforced solids. Their contribution to the strain energy is modeled using a pair of preferred directions identified in the reference configuration, and from which structure tensors characterizing the anisotropy are formed. The model is *structural* in the sense that it involves two layers and within each layer information about the orientations of the collagen fibers, obtained from a statistical analysis of histological sections of each arterial layer (see Holzapfel et al. [27]), is incorporated. The material parameters

included in the model, although phenomenologically based, reflect the structural characteristics within each arterial layer. The properties of the matrix material are described in terms of a single material constant and those of the fiber bundles by two additional constants in each layer.

With a specific form of the model used for illustrative purposes, the predictions of the model are examined in detail and compared with those from some phenomenological models. The predictions of the model agree well with the typical mechanical response of arteries observed in experiments. The Cauchy stress distributions through the deformed arterial wall in the physiological state are also determined in order to illustrate the significant difference made by incorporation of the residual stresses. Moreover, the three-dimensional model introduced here is consistent with the convexity requirements that ensure mechanically and mathematically reliable behavior. It also admits an efficient numerical implementation within the finite element method, an aspect which is discussed in detail in [26], in which there is an extension to viscoelasticity (suitable for the modeling of muscular arteries). Extension to elastoplasticity is discussed in [20] and [21]. Thus, more complex boundary-value problems, possibly of clinical relevance, can be solved on the basis of the proposed model.

Section 6 contains a summary of the results and concludes with an assessment of the advantages of the new model.

2. Histology and Typical Mechanical Behavior of Arterial Walls

Efficient constitutive descriptions of arterial walls require a fundamental knowledge and understanding of the entire arterial histology, i.e. the morphological structure, and an extensive investigation of the particular arterial wall of interest. Additionally, this is of crucial importance for the understanding of the general mechanical characteristics of arterial walls and the components that provide the main contributions to the deformation process.

This brief overview is included only for the purpose of clarifying the macroscopic and microscopic structure of arterial walls and to provide essential information for scientists without a background in biology or physiology. For a more detailed exposition of the different mechanical characteristics of the interrelated arterial components and the overall functioning of the blood vessel (which constitutive models aim to characterize) see, for example, the reviews by Rhodin [48] and Silver et al. [54].

2.1. ARTERIAL HISTOLOGY

This paper is concerned with the *in vitro* passive behavior of arteries. Hence, *in vivo* effects such as the vasa vasorum, nerve control, humoral control, perivascular connective tissue, etc. and neighboring organs such as the pulsating heart are not relevant and are not therefore discussed here.

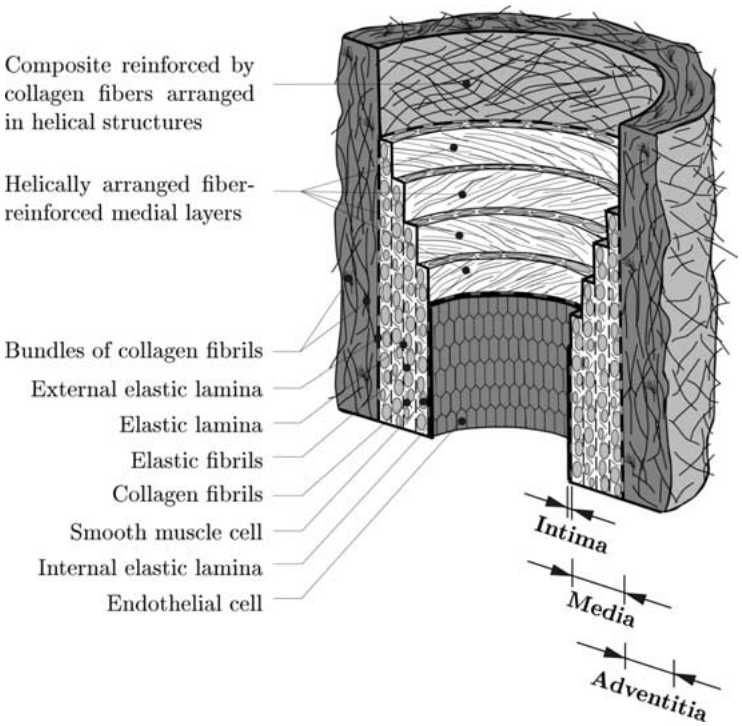

Figure 1. Diagrammatic model of the major components of a healthy *elastic* artery composed of three layers: intima (I), media (M), adventitia (A). I is the innermost layer consisting of a single layer of endothelial cells that rests on a thin basal membrane and a subendothelial layer whose thickness varies with topography, age and disease. M is composed of smooth muscle cells, a network of elastic and collagen fibrils and elastic laminae which separate M into a number of fiber-reinforced layers. The primary constituents of A are thick bundles of collagen fibrils arranged in helical structures; A is the outermost layer surrounded by loose connective tissue.

In general, arteries are roughly subdivided into two types: *elastic* and *muscular*. Elastic arteries have relatively large diameters and are located close to the heart (for example, the aorta and the carotid and iliac arteries), while muscular arteries are located at the periphery (for example, femoral, celiac, cerebral arteries). However, some arteries exhibit morphological structures of both types. Here we focus attention on the microscopic structure of arterial walls composed of three distinct layers, the *intima* (*tunica intima*), the *media* (*tunica media*) and the *adventitia* (*tunica externa*). We discuss the constituents of arterial walls from the mechanical perspective and emphasize those aspects which are important to researchers interested in constitutive issues. Figure 1 shows a model of a healthy elastic artery.

2.1.1. *Intima*

The intima is the innermost layer of the artery. It consists of a single layer of endothelial cells lining the arterial wall and resting on a thin basal membrane (basal lamina). There is also a subendothelial layer whose thickness varies with topography, age and disease. In healthy young muscular arteries, however, the subendothelial layer is almost non-existent. In healthy young individuals the intima is very thin and makes an insignificant contribution to the *solid* mechanical properties of the arterial wall. However, it should be noted that the intima thickens and stiffens with age (*arteriosclerosis*) so that the mechanical contribution may become significant.

It is known that pathological changes of the intimal components may be associated with *atherosclerosis*, the most common disease of arterial walls. It involves deposition of fatty substances, calcium, collagen fibers, cellular waste products and fibrin (a clotting material in the blood). The resulting build-up is called *atherosclerotic* plaque. It may be very complex in geometry and biochemical composition. In later stages the media is also affected. These pathological changes are associated with significant alterations in the mechanical properties of the arterial wall. Hence, the mechanical behavior of atherosclerotic arteries differs significantly from that of healthy arteries.

2.1.2. *Media*

The media is the middle layer of the artery and consists of a complex three-dimensional network of smooth muscle cells, and elastin and collagen fibrils. According to [48] the fenestrated elastic laminae separate the media into a varying number of well-defined concentrically fiber-reinforced medial layers. The number of elastic laminae decreases toward the periphery (as the size of the vessels decreases) so that elastic laminae are hardly present in muscular arteries.

The media is separated from the intima and adventitia by the so-called internal elastic lamina and external elastic lamina (absent in cerebral blood vessels), respectively. In muscular arteries these laminae appear as prominent structures, whereas in elastic arteries they are hardly distinguishable from the regular elastic laminae. The orientation of and close interconnection between the elastic and collagen fibrils, elastic laminae, and smooth muscle cells together constitute a continuous fibrous helix (Faserschraube) [52, 58]. The helix has a small pitch so that the fibrils in the media are almost circumferentially oriented. This structured arrangement gives the media high strength, resilience and the ability to resist loads in both the longitudinal and circumferential directions. From the mechanical perspective, the media is the most significant layer in a healthy artery.

2.1.3. *Adventitia*

The adventitia is the outermost layer of the artery and consists mainly of fibroblasts and fibrocytes (cells that produce collagen and elastin), histological ground

substance and thick bundles of collagen fibrils forming a fibrous tissue. The adventitia is surrounded continuously by loose connective tissue. The thickness of the adventitia depends strongly on the type (elastic or muscular) and the physiological function of the blood vessel and its topographical site. For example, in cerebral blood vessels there is virtually no adventitia.

The wavy collagen fibrils are arranged in helical structures and serve to reinforce the wall. They contribute significantly to the stability and strength of the arterial wall. The adventitia is much less stiff in the load-free configuration and at low pressures than the media. However, at higher levels of pressure the collagen fibers reach their straightened lengths and the adventitia changes to a stiff 'jacket-like' tube which prevents the artery from overstretch and rupture.

2.2. TYPICAL MECHANICAL BEHAVIOR OF ARTERIAL WALLS

Each constitutive framework and its associated set of material parameters requires detailed studies of the particular material of interest. Its reliability is strongly related to the quality and completeness of available experimental data, which may come from appropriate *in vivo* tests or from *in vitro* tests that mimic real loading conditions in a physiological environment.

In vivo tests seem to be preferable because the vessel is observed under real life conditions. However, *in vivo* tests have major limitations because of, for example, the influence of hormones and nerval control. Moreover, data sets from the complex material response of arterial walls subject to simultaneous cyclic *inflation*, axial *extension* and *twist* can only be measured in an *in vitro* experiment. Only with such data sets can the anisotropic mechanical behavior of arterial walls be described completely. In addition, in *in vitro* experiments the contraction state (active or passive) of the muscular media has to be determined. This can be done with appropriate chemical agents.

For pure inflation tests of straight artery tubes, which is the most common two-dimensional test, see the early work [2] (in which shear deformations are not considered). Since arteries do not change their volume within the physiological range of deformation [4], they can be regarded as incompressible materials. Hence, by means of the incompressibility constraint we may determine the mechanical properties of three-dimensional specimens from two-dimensional tests [36]. It is important to note that uniaxial extension tests on arterial patches (strips) provide basic information about the material [24] but they are certainly not sufficient to quantify completely the anisotropic behavior of arterial walls. Other uniaxial extension tests on small arterial rings (so-called ring tests) are also insufficient [9]. In general, a segment of vessel shortens on removal from the body, as was first reported in [15]. The *in vivo* pre-stretch in the longitudinal direction must therefore be reproduced within *in vitro* tests [37].

Each non-axisymmetric arterial segment (such as a bifurcation or a segment with sclerotic changes) under combined inflation and axial extension develops

significant shear stresses in the wall. Hence, in order to characterize the shear properties of arterial walls shear tests are required. In shear tests *either* the angle of twist of an arterial tube subjected to transmural pressure, longitudinal force and torque [12] *or* the shear deformation of a rectangular arterial wall specimen subjected to shear forces [65] is measured. Additionally, one can classify mechanical tests according to the strain rates used (quasi-static or dynamic) and to whether the loading is performed cyclically or discontinuously (creep and relaxation tests). It has been known for many years that the load-free configuration of an artery is not a stress-free state [61]. In general, a load-free arterial ring contains residual stresses. It is of crucial importance to identify these in order to predict reliably the state of stress in an arterial wall, and this has been the aim of many experimental investigations (see, for example, the bending tests on blood vessel walls in [68]).

The mechanical behavior of arteries depends on physical and chemical environmental factors, such as temperature, osmotic pressure, pH, partial pressure of carbon dioxide and oxygen, ionic concentrations and monosaccharide concentration. In *ex vivo* conditions the mechanical properties are altered due to biological degradation. Therefore, arteries should be tested in appropriate oxygenated, temperature controlled salt solutions as fresh as possible. For an overview of experimental test methods used to verify material parameters, see [32] and the references contained therein.

As indicated in Section 2.1 the composition of arterial walls varies along the arterial tree. Hence, there seems to be a systematic dependence of the shape of the stress–strain curve for a blood vessel on its anatomical site. This fact has been demonstrated several times experimentally; see, for example, the early works [51, 37] and [8]. Although the mechanical properties of arterial walls vary along the arterial tree, the general mechanical characteristics exhibited by arterial walls are the same. In order to explain the typical stress–strain response of an arterial wall of smooth muscles in the passive state (governed mainly by elastin and collagen fibers), we refer to Figure 2. Note that the curves in Figure 2 are schematic, but based on experimental tension tests performed in the authors' laboratory (some of which is described in a recent paper [28]).

As can be seen, a circumferential strip of the media subjected to uniaxial cyclic loading and unloading typically displays pronounced stress softening, which occurs during the first few load cycles. The stress softening effect diminishes with the number of load cycles until the material exhibits a *nearly repeatable* cyclic behavior, and hence the biological material is said to be 'pre-conditioned' (compare with, for example, the characteristic passive behavior of a bovine coronary artery in [32], p. 33). Thus, depending on the type of artery considered, the material behavior may be regarded as (perfectly) elastic for proximal arteries of the elastic type, or viscoelastic for distal arteries of the muscular type, often modeled as pseudoelastic (see, for example, [18]). For a definition of the term *pseudoelasticity* in the context of biomechanics the reader is referred to [18].

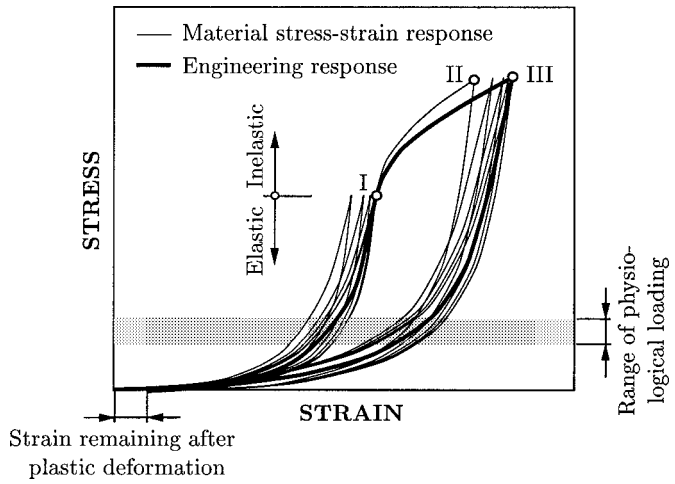

Figure 2. Schematic diagram of typical uniaxial stress–strain curves for circumferential arterial strips (from the media) in passive condition (based on tension tests performed in the authors' laboratory): cyclic loading and unloading, associated with stress softening effects, lead to a pre-conditioned material which behaves (perfectly) elastically or viscoelastically (nearly repeatable cyclic behavior) – point I. Loading beyond the (visco)elastic domain up to point II leads to inelastic deformations. Additional loading and unloading cycles display stress softening again until point III is reached. Then the material exhibits (perfectly) elastic or viscoelastic response. The thick solid line indicates the (approximate) engineering response of the material.

Healthy arteries are highly deformable composite structures and show a nonlinear stress–strain response with a typical (exponential) stiffening effect at higher pressures, as illustrated in Figure 2. This stiffening effect, common to all biological tissues, is based on the recruitment of the embedded (load carrying) wavy collagen fibrils, which leads to the characteristic anisotropic mechanical behavior of arteries; see the classical works [49, 40]. Early works on arterial anisotropy (see, for example, [45]) considered arterial walls to be cylindrically orthotropic, which is generally accepted in the literature.

Loading beyond the (visco)elastic domain (indicated by point I in Figure 2), far outside the physiological range of deformation, often occurs during mechanical treatments such as percutaneous transluminal angioplasty. This procedure involves dilation of an artery using a balloon catheter (see [3]). In the strain range up to point II in Figure 2, the deformation process in an arterial layer is associated with inelastic effects (elastoplastic and/or damage mechanisms) leading to significant changes in the mechanical behavior (see [44, 28] and [21]). This overstretching involves dissipation, which is represented by the area between the loading and unloading curves. Hence, starting from point II, additional cyclic loading and unloading again displays stress softening, which diminishes with the number of load cycles. At point III the material exhibits a (perfectly) elastic or viscoelastic behavior. However, unloading initiated from point III returns the arterial (medial) strip to

an unstressed state with non-vanishing strains remaining, these being responsible for the change of shape. With preconditioning effects neglected, the thick solid line in Figure 2 indicates the (approximate) engineering response associated with the actual physical behavior.

The model proposed in Section 5 is intended to capture only the elastic portion of the curves in Figure 2, i.e. up to point I. For the remaining portions of the curves a rate-independent elastoplastic model and the associated algorithmic formulation and finite element implementation was recently proposed in [20].

3. Continuum-Mechanical Framework

In this section we summarize the equations that provide the general continuum description of the deformation and the hyperelastic stress response of the material. As a basis for reporting the performance of different constitutive models for arteries we consider the mechanical response of a thick-walled circular cylindrical tube under various boundary loads. We specify the strain measures to be used and discuss the equilibrium equation which arises in the considered problem. We also give expressions for the torsional couple and the reduced axial force acting on the tube, these being crucial for the subsequent comparative study of constitutive models.

3.1. FINITE HYPERELASTICITY

3.1.1. *Description of the Deformation*

Let Ω_0 be a (fixed) reference configuration of the continuous body of interest (assumed to be stress-free). We use the notation $\boldsymbol{\chi} : \Omega_0 \to \mathbb{R}^3$ for the deformation, which transforms a typical material point $\mathbf{X} \in \Omega_0$ to a position $\mathbf{x} = \boldsymbol{\chi}(\mathbf{X}) \in \Omega$ in the deformed configuration, denoted Ω. Further, let $\mathbf{F}(\mathbf{X}) = \partial \boldsymbol{\chi}(\mathbf{X})/\partial \mathbf{X}$ be the deformation gradient and $J(\mathbf{X}) = \det \mathbf{F} > 0$ the local volume ratio.

Following [14] and [41], we consider the multiplicative decomposition

$$\mathbf{F} = (J^{1/3}\mathbf{I})\overline{\mathbf{F}} \tag{1}$$

of $\mathbf{F}$ into spherical (dilatational) and unimodular (distortional) parts. We use the right and left Cauchy–Green tensors, denoted $\mathbf{C}$ and $\mathbf{b}$ respectively, and their modified counterparts, denoted $\overline{\mathbf{C}}$ and $\overline{\mathbf{b}}$ respectively, associated with $\overline{\mathbf{F}}$. From equation (1) we then have

$$\mathbf{C} = \mathbf{F}^{\mathrm{T}}\mathbf{F} = J^{2/3}\overline{\mathbf{C}}, \qquad \overline{\mathbf{C}} = \overline{\mathbf{F}}^{\mathrm{T}}\overline{\mathbf{F}}, \tag{2}$$

$$\mathbf{b} = \mathbf{F}\mathbf{F}^{\mathrm{T}} = J^{2/3}\overline{\mathbf{b}}, \qquad \overline{\mathbf{b}} = \overline{\mathbf{F}}\,\overline{\mathbf{F}}^{\mathrm{T}}. \tag{3}$$

In addition, we introduce the Green–Lagrange strain tensor $\mathbf{E}$, and, through equation (1), its associated modified strain measure $\overline{\mathbf{E}}$. Thus,

$$\mathbf{E} = \frac{1}{2}(\mathbf{C} - \mathbf{I}) = J^{2/3}\overline{\mathbf{E}} + \frac{1}{2}(J^{2/3} - 1)\mathbf{I}, \qquad \overline{\mathbf{E}} = \frac{1}{2}(\overline{\mathbf{C}} - \mathbf{I}), \tag{4}$$

where $\mathbf{I}$ denotes the second-order unit tensor.

3.1.2. *Hyperelastic Stress Response*

In order to describe the hyperelastic stress response of arterial walls, we employ a set $\{\mathbf{A}_\alpha \mid \alpha = 1, \ldots, n\}$ of (second-order) tensors which characterize the wall structure, and we postulate the existence of a Helmholtz free-energy function $\Psi(\mathbf{E}, \mathbf{A}_1, \ldots, \mathbf{A}_n)$. Subsequently, we assume the *decoupled* form

$$\Psi(\mathbf{E}, \mathbf{A}_1, \ldots, \mathbf{A}_n) = U(J) + \overline{\Psi}(\overline{\mathbf{E}}, \mathbf{A}_1, \ldots, \mathbf{A}_n), \tag{5}$$

where the function U is a purely volumetric contribution and $\overline{\Psi}$ is a purely isochoric contribution to the free energy Ψ.

From the Clausius–Planck inequality, standard arguments lead to the well-known equation $\mathbf{S} = \partial\Psi(\mathbf{E}, \mathbf{A}_1, \ldots, \mathbf{A}_n)/\partial\mathbf{E}$ for the second Piola–Kirchhoff stress. Equation (5) then gives

$$\mathbf{S} = \mathbf{S}_{\text{vol}} + \overline{\mathbf{S}} \quad \text{with } \mathbf{S}_{\text{vol}} = \frac{\partial U(J)}{\partial \mathbf{E}},\ \overline{\mathbf{S}} = \frac{\partial \overline{\Psi}(\overline{\mathbf{E}}, \mathbf{A}_1, \ldots, \mathbf{A}_n)}{\partial \mathbf{E}}. \tag{6}$$

We shall also require the standard results

$$\frac{\partial J}{\partial \mathbf{E}} = J\mathbf{C}^{-1} \quad \text{and} \quad \frac{\partial \overline{\mathbf{E}}}{\partial \mathbf{E}} = J^{-2/3}\left(\mathbb{I} - \frac{1}{3}\overline{\mathbf{C}} \otimes \overline{\mathbf{C}}^{-1}\right) \tag{7}$$

from tensor analysis (see, for example, [25]), where $\mathbb{I}$ denotes the fourth-order identity tensor which, in index notation, has the form $(\mathbb{I})_{IJKL} = (\delta_{IK}\delta_{JL} + \delta_{IL}\delta_{JK})/2$, δ_{IJ} being the Kronecker delta. With these results, equations $(6)_2$ and $(6)_3$ become, after some straightforward tensor manipulations and the introduction of the hydrostatic pressure $p = \mathrm{d}U/\mathrm{d}J$ as in [25],

$$\mathbf{S}_{\text{vol}} = pJ\mathbf{C}^{-1}, \qquad \overline{\mathbf{S}} = J^{-2/3}\text{Dev}\left(\frac{\partial \overline{\Psi}}{\partial \overline{\mathbf{E}}}\right). \tag{8}$$

The operator $\text{Dev}(\bullet)$ in (8) is defined by

$$\text{Dev}(\bullet) = (\bullet) - \frac{1}{3}[(\bullet) : \overline{\mathbf{C}}]\overline{\mathbf{C}}^{-1}, \tag{9}$$

and furnishes the physically correct deviatoric operator in the Lagrangian description, so that $\text{Dev}(\bullet) : \mathbf{C} = 0$. Note that in the description of an incompressible material (which an artery is assumed to be) the hydrostatic pressure p becomes an indeterminate *Lagrange multiplier*.

A Piola transformation of equations (8) enables the Cauchy stress tensor $\boldsymbol{\sigma} = J^{-1}\mathbf{F}\mathbf{S}\mathbf{F}^{\mathrm{T}}$ to be put in the *decoupled* form

$$\boldsymbol{\sigma} = \boldsymbol{\sigma}_{\text{vol}} + \overline{\boldsymbol{\sigma}} \quad \text{with } \boldsymbol{\sigma}_{\text{vol}} = p\mathbf{I},\ \overline{\boldsymbol{\sigma}} = J^{-1}\text{dev}\left(\overline{\mathbf{F}}\frac{\partial \overline{\Psi}}{\partial \overline{\mathbf{E}}}\overline{\mathbf{F}}^{\mathrm{T}}\right), \tag{10}$$

analogously to equation (8), where the operator $\text{dev}(\bullet)$ is defined by

$$\text{dev}(\bullet) = (\bullet) - \frac{1}{3}[(\bullet) : \mathbf{I}]\mathbf{I}. \tag{11}$$

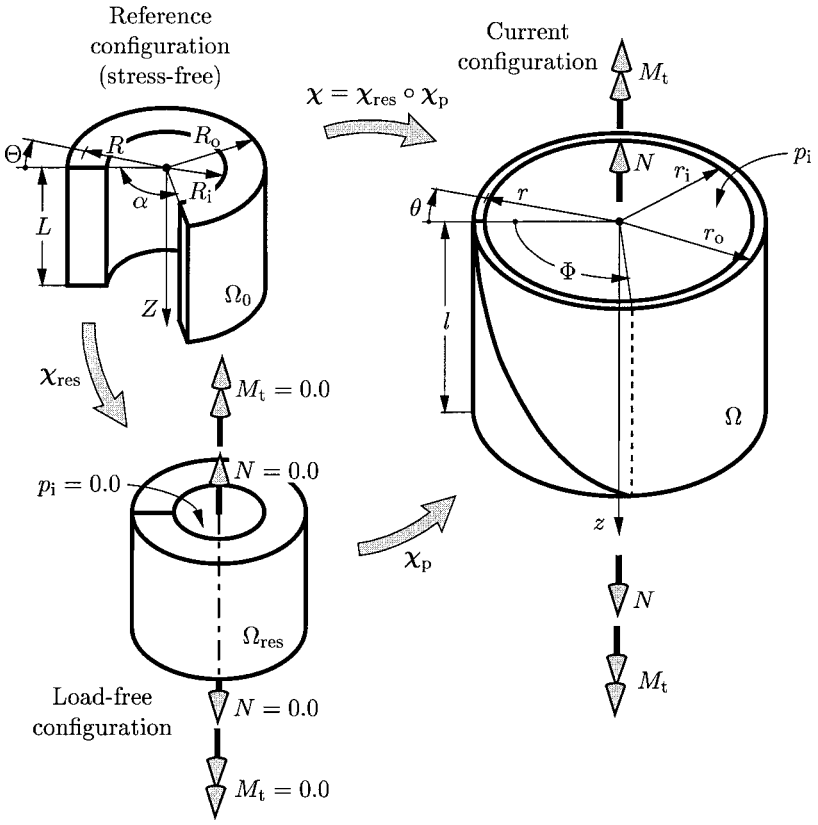

Figure 3. Arterial ring in the the (stress-free) reference configuration Ω_0, the load-free configuration Ω_{res} and the current configuration Ω.

It furnishes the physically correct deviatoric operator in the Eulerian description, so that $\text{dev}(\bullet) : \mathbf{I} = 0$.

3.2. COMBINED BENDING, INFLATION, EXTENSION AND TORSION OF A TUBE

3.2.1. *Basic Kinematics*

We consider the artery as an incompressible thick-walled cylindrical tube subjected to various loads. It is known that the load-free configuration, Ω_{res} say, in which the artery is excised from the body and *not* subjected to any loads is not a stress-free (or strain-free) reference configuration Ω_0. Thus, the arterial ring springs open when cut in a radial direction. It appears that Vaishnav and Vossoughi [61] were the first to publish this finding. Bearing in mind the statement in Section 1, we *assume* that the open sector is the undeformed (stress-free and fixed) reference configuration Ω_0, as depicted in Figure 3.

Thus, in terms of cylindrical polar coordinates (R, Θ, Z), the geometrical region Ω_0 of the tube is defined by

$$R_\mathrm{i} \leqslant R \leqslant R_\mathrm{o}, \qquad 0 \leqslant \Theta \leqslant (2\pi - \alpha), \qquad 0 \leqslant Z \leqslant L, \tag{12}$$

where R_i, R_o, α and L denote the inner and outer radii, the opening angle and length of the undeformed (split) tube, respectively. Note that the opening angle α identified in Figure 3 differs from the definition normally used (see, for example, Fung and Liu [19]).

The deformation $\boldsymbol{\chi}$ takes Ω_0 into the current configuration Ω. For the considered problem $\boldsymbol{\chi} = \boldsymbol{\chi}_\mathrm{p} \circ \boldsymbol{\chi}_\mathrm{res}$ is the composition of the deformations $\boldsymbol{\chi}_\mathrm{res}$ and $\boldsymbol{\chi}_\mathrm{p}$, as indicated in Figure 3, where $\boldsymbol{\chi}_\mathrm{res}$ generates the load-free configuration Ω_res associated with residual stresses, while $\boldsymbol{\chi}_\mathrm{p}$ is associated with inflation, axial elongation and torsion of the tube, and leads to the final configuration Ω. It is important to note that the residually stressed configuration Ω_res of an artery arises from certain growth mechanisms of the different layers, and hence, in general, the residually stressed state is more complex than considered here. For discussion of stress-dependent growth and remodeling we refer to, for example, Rodriguez et al. [50] and Rachev [46]. It may also be noted that it has been found that residual stress accumulates due to cyclic loading in two-phase models of soft tissue *without* growth (see, for example, Huyghe et al. [34]).

In terms of cylindrical polar coordinates (r, θ, z), the geometry of the deformed configuration Ω is given by

$$r_\mathrm{i} \leqslant r \leqslant r_\mathrm{o}, \qquad 0 \leqslant \theta \leqslant 2\pi, \qquad 0 \leqslant z \leqslant l, \tag{13}$$

where r_i, r_o and l denote the inner and outer radii and the length of the deformed tube, respectively.

The deformation $\boldsymbol{\chi}$, which is taken to be isochoric, may then be written in the form

$$\boldsymbol{\chi} = r\mathbf{e}_r + z\mathbf{e}_z \tag{14}$$

with reference to the (unit) basis vectors $\{\mathbf{e}_r, \mathbf{e}_\theta, \mathbf{e}_z\}$ associated with the cylindrical polar coordinates (r, θ, z), where

$$r = \sqrt{\frac{R^2 - R_\mathrm{i}^2}{k\lambda_z} + r_\mathrm{i}^2}, \qquad \theta = k\Theta + Z\frac{\Phi}{L}, \qquad z = \lambda_z Z, \tag{15}$$

λ_z is the (constant) axial stretch, the parameter k, defined by $k = 2\pi/(2\pi - \alpha)$, is a convenient measure of the tube opening angle in the unstressed configuration, r_i is the inner radius in the deformed configuration and Φ is the angle of twist of the tube arising from the torsion.

In addition to λ_z, it is convenient to introduce the notations defined by

$$\lambda_r(R) = \frac{\partial r}{\partial R} = \frac{R}{rk\lambda_z}, \qquad \lambda_\theta(R) = \frac{r}{R}\frac{\partial \theta}{\partial \Theta} = \frac{kr}{R},$$
$$\gamma(R) = r\frac{\partial \theta}{\partial z} = r\frac{\Phi}{l}. \tag{16}$$

Here $\lambda_r(R)$, $\lambda_\theta(R)$ and λ_z are the principal stretches of the deformation associated with the radial, circumferential and axial directions *when there is no twist*, while $\gamma(R)$, which is associated with the twist, represents locally the amount of shear in a (θ, z)-plane. Since each of these quantities depends only on the radius R, the one-dimensional character of the problem is apparent. When $\gamma \neq 0$, λ_r is the principal stretch in the radial direction but λ_θ and λ_z are not then principal stretches. The condition that the volume is preserved during the deformation is independent of γ and requires simply that

$$\lambda_r \lambda_\theta \lambda_z = 1. \tag{17}$$

Note that

$$r_{\mathrm{i}} = \lambda_{\theta \mathrm{i}} \frac{R_{\mathrm{i}}}{k}, \tag{18}$$

where $\lambda_{\theta\,\mathrm{i}}$ denotes the value of λ_θ at the inner surface of the tube.

The first term $k\Theta$ in $(15)_2$ represents the deformation from configuration Ω_0 to Ω_{res} while the second term $Z\Phi/L$ describes the influence of the torsion. In terms of the parameters k, $\lambda_{\theta \mathrm{i}}$, λ_z and Φ, equations (15), (18) define the combined bending, inflation, axial extension and torsion of a thick-walled tube.

On use of (17), the deformation gradient $\mathbf{F}$, referred to cylindrical polar coordinates, may be expressed in the form

$$\mathbf{F} = \overline{\mathbf{F}} = (\lambda_\theta \lambda_z)^{-1} \mathbf{e}_r \otimes \mathbf{E}_R + \lambda_\theta\, \mathbf{e}_\theta \otimes \mathbf{E}_\Theta + \gamma \lambda_z\, \mathbf{e}_\theta \otimes \mathbf{E}_Z + \lambda_z\, \mathbf{e}_z \otimes \mathbf{E}_Z, \tag{19}$$

where $\{\mathbf{E}_R, \mathbf{E}_\Theta, \mathbf{E}_Z\}$ is the set of unit cylindrical polar basis vectors associated with (R, Θ, Z). Note that $\mathbf{E}_Z = \mathbf{e}_z$.

Use of equations (2), (3) enables the Cauchy–Green tensors to be given in terms of cylindrical polar coordinates. Thus,

$$\begin{aligned} \mathbf{C} = \overline{\mathbf{C}} \;=\; & (\lambda_\theta \lambda_z)^{-2} \mathbf{E}_R \otimes \mathbf{E}_R + \lambda_\theta^2\, \mathbf{E}_\Theta \otimes \mathbf{E}_\Theta + \lambda_z^2 (1 + \gamma^2)\, \mathbf{E}_Z \otimes \mathbf{E}_Z \\ & + \gamma \lambda_\theta \lambda_z (\mathbf{E}_\Theta \otimes \mathbf{E}_Z + \mathbf{E}_Z \otimes \mathbf{E}_\Theta), \end{aligned} \tag{20}$$

$$\begin{aligned} \mathbf{b} = \overline{\mathbf{b}} \;=\; & (\lambda_\theta \lambda_z)^{-2} \mathbf{e}_r \otimes \mathbf{e}_r + (\lambda_\theta^2 + \gamma^2 \lambda_z^2) \mathbf{e}_\theta \otimes \mathbf{e}_\theta + \lambda_z^2\, \mathbf{e}_z \otimes \mathbf{e}_z \\ & + \gamma \lambda_z^2 (\mathbf{e}_\theta \otimes \mathbf{e}_z + \mathbf{e}_z \otimes \mathbf{e}_\theta). \end{aligned} \tag{21}$$

The deformation gradient (19) and the Cauchy–Green tensors (20) and (21) play a crucial role in the derivation of the state of stress in an arterial wall. A more general deformation including azimuthal and axial shear is discussed in the paper by Guccione et al. [22].

3.2.2. *Equilibrium Equations*

In the absence of body forces the equilibrium equations are

$$\operatorname{div} \boldsymbol{\sigma} = \mathbf{0}, \tag{22}$$

where div(•) denotes the spatial divergence of the spatial tensor field (•). Note that in cylindrical polar coordinates (r, θ, z), because of the geometrical and constitutive symmetry, the only non-trivial component of (22) is

$$\frac{\mathrm{d}\sigma_{rr}}{\mathrm{d}r} + \frac{(\sigma_{rr} - \sigma_{\theta\theta})}{r} = 0 \tag{23}$$

(see, for example, [42]). From this equation and the boundary condition $\sigma_{rr}|_{r=r_\mathrm{o}} = 0$ on the outer surface of the tube, the radial Cauchy stress σ_{rr} may be calculated as

$$\sigma_{rr}(\xi) = \int_{\xi}^{r_\mathrm{o}} (\sigma_{rr} - \sigma_{\theta\theta}) \frac{\mathrm{d}r}{r}, \quad r_\mathrm{i} \leqslant \xi \leqslant r_\mathrm{o}. \tag{24}$$

The internal pressure $p_\mathrm{i} = -\sigma_{rr}|_{r=r_\mathrm{i}}$ is then obtained in the form

$$p_\mathrm{i} = \int_{r_\mathrm{i}}^{r_\mathrm{o}} (\sigma_{\theta\theta} - \sigma_{rr}) \frac{\mathrm{d}r}{r}. \tag{25}$$

This equation plays an important role in the numerical solution of the problem considered.

When the state of deformation is known, expressions for the axial force N and the torsional couple M_t can be calculated via the definitions

$$N = 2\pi \int_{r_\mathrm{i}}^{r_\mathrm{o}} \sigma_{zz}\, r\,\mathrm{d}r, \qquad M_\mathrm{t} = 2\pi \int_{r_\mathrm{i}}^{r_\mathrm{o}} \sigma_{\theta z} r^2\,\mathrm{d}r. \tag{26}$$

In view of the additive split of the Cauchy stress tensor $\boldsymbol{\sigma}$ into volumetric and isochoric parts introduced in $(10)_1$, we may recast equations (25) and $(26)_2$ by using the decompositions $\sigma_{\theta\theta} = p + \overline{\sigma}_{\theta\theta}$ and $\sigma_{rr} = p + \overline{\sigma}_{rr}$ to obtain

$$p_\mathrm{i} = \int_{r_\mathrm{i}}^{r_\mathrm{o}} (\overline{\sigma}_{\theta\theta} - \overline{\sigma}_{rr}) \frac{\mathrm{d}r}{r}, \qquad M_\mathrm{t} = 2\pi \int_{r_\mathrm{i}}^{r_\mathrm{o}} \overline{\sigma}_{\theta z} r^2\,\mathrm{d}r, \tag{27}$$

where $\overline{\sigma}_{\theta\theta}$, $\overline{\sigma}_{rr}$ denote the isochoric parts of the normal components of (Cauchy) stress in the circumferential and radial directions, while $\overline{\sigma}_{\theta z} = \sigma_{\theta z}$ is the shear component of (Cauchy) stress acting tangentially to the cross-section of the tube.

Use of the additive split (10) and equation (24) enables the axial force N in equation $(26)_1$ to be expressed as

$$N = 2\pi \int_{r_\mathrm{i}}^{r_\mathrm{o}} \left[\int_{r_\mathrm{o}}^{\xi} (\overline{\sigma}_{\theta\theta} - \overline{\sigma}_{rr}) \frac{\mathrm{d}r}{r} - \overline{\sigma}_{rr} + \overline{\sigma}_{zz} \right] \xi\,\mathrm{d}\xi. \tag{28}$$

Reversal of the order of integration in (28) and use of the expression $(27)_1$ leads to the general formula

$$F = \pi \int_{r_\mathrm{i}}^{r_\mathrm{o}} (2\overline{\sigma}_{zz} - \overline{\sigma}_{\theta\theta} - \overline{\sigma}_{rr}) r\,\mathrm{d}r \tag{29}$$

for the *reduced axial force* $F = N - r_{\mathrm{i}}^2 \pi p_{\mathrm{i}}$. This expression for F is very important since it gives precisely the force that is measured during inflation tests on arteries. A specific form of equation (29) is given in equation (15) of [5]. In subsequent sections of the present paper equations (27) and (29) will be specialized for several constitutive models that have been used in the literature to represent the mechanical response of arteries.

REMARK 3.1. For a thin-walled cylindrical tube we make the simplification $\sigma_{rr} = p + \overline{\sigma}_{rr} = 0$ for the radial stress (the membrane approximation). On use of $\sigma_{\theta\theta} = p + \overline{\sigma}_{\theta\theta}$ and $\overline{\sigma}_{\theta z} = \sigma_{\theta z}$, equations $(27)_1$, $(27)_2$ and (29) then enable the reduced equations for the internal pressure p_{i}, the torsional couple M_{t} and the reduced axial force F to be given simply as

$$p_{\mathrm{i}} = \frac{h}{r}\sigma_{\theta\theta}, \qquad M_{\mathrm{t}} = 2\pi r^2 h \sigma_{\theta z}, \qquad F = \pi r h (2\sigma_{zz} - \sigma_{\theta\theta}), \tag{30}$$

where r and h denote the radius and wall thickness of the deformed tube, respectively. It is important to note that with this membrane approximation the contribution $\boldsymbol{\chi}_{\mathrm{res}}$ to the deformation is inadmissible and residual stresses cannot be included.

REMARK 3.2. Here we describe briefly the numerical technique used in the solution of the problem of bending, axial extension, inflation and torsion of a thick-walled cylindrical tube.

By assuming a particular state of residual strain (characterized by the parameter k), the fixed axial stretch λ_z and fixed angle of twist Φ of the tube, the isochoric part of the strain (and hence the stress) can always be expressed in terms of the two variables $\lambda_{\theta\mathrm{i}}$ and r, i.e. the circumferential stretch at the inner surface of the tube and the radius, respectively. Hence, the equation of equilibrium $(27)_1$ may be written in the general form

$$p_{\mathrm{i}} = \int_{r_{\mathrm{i}}}^{r_{\mathrm{o}}} \mathcal{F}(\lambda_{\theta\,\mathrm{i}}, r)\frac{\mathrm{d}r}{r}, \tag{31}$$

where r_{i} is given in terms of $\lambda_{\theta\mathrm{i}}$ by (18). Since closed-form evaluation of equation (31) is only possible for very simple constitutive equations, we employ a *Gaussian integration scheme* [31], i.e.

$$p_{\mathrm{i}} \approx \sum_{j=1}^{n} \mathcal{F}(\lambda_{\theta\mathrm{i}}, r_j)\frac{w_j}{r_j}, \tag{32}$$

where w_j and r_j $(j = 1, \ldots, n)$, denote the weights and the Gaussian points, and n is the order of integration. Equation (32) is, in general, nonlinear in the single unknown $\lambda_{\theta\mathrm{i}}$, and, for given p_{i}, can be solved for $\lambda_{\theta\mathrm{i}}$ using, for example, a standard *Newton iteration* with the initial value $\lambda_{\theta\mathrm{i}} = 1.0$.

Since the deformation is now determined, the torsional couple M_t and the reduced axial force F follow directly from equations $(27)_2$ and (29), respectively. This computation is carried out by employing another *Gaussian integration*. It turns out that for the considered range of deformations a three-point integration ($n = 3$) with the accuracy of order five gives sufficiently accurate solutions.

REMARK 3.3. The theory described above is designed to capture the deformation behavior in the central part of a tube so as to exclude end effects. Therefore, axial dependence of the deformation is not considered. This reflects the typical setting used in experiments (see, for example, [18] or [53], amongst others).

4. Some Constitutive Models for Arterial Walls

The *active* mechanical behavior of arterial walls is governed mainly by the intrinsic properties of elastin and collagen fibers and by the degree of activation of smooth muscles. An adequate constitutive model for arteries which incorporates the active state (contraction of smooth muscles) was proposed recently by Rachev and Hayashi [47].

The *passive* mechanical behavior of arterial walls is quite different and is governed mainly by the elastin and collagen fibers (see, for example, [8]). The passive state of the smooth muscles may also contribute to the passive arterial behavior but the extent of this contribution is not yet known. Most constitutive models proposed for arteries are valid for the passive state of smooth muscles and are based on a phenomenological approach which describes the artery as a macroscopic system. Furthermore, most of these models were designed to capture the response near the physiological state and in this respect they have been successfully applied in fitting experimental data. The most common potentials (strain-energy functions) are of exponential type, although polynomial and logarithmic forms are also used. For a review of a number of constitutive models describing the overall passive behavior, see Humphrey [32].

Some of the constitutive models proposed use the biphasic theory to describe arterial walls as hydrated soft tissues; see, for example, the works by Simon and co-workers [56, 55]. Less frequently used are models which account for the specific morphological structure of arterial walls. One attempt to model the helically wound fibrous structure is provided by Tözeren [60], which is based on the idea that the only wall constituent is the fiber structure. However, this is a significant simplification of the histological structure.

Another structural model due to Wuyts et al. [67] assumes that the wavy collagen fibrils are embedded in concentrically arranged elastin/smooth-muscle membranes, which is in agreement with the histological situation [49]. The model in [67] assumes that the collagen fibrils have a statistically distributed initial length. Each fibril may be stretched initially with a very low force but thereafter its behavior is

linearly elastic. Only the media is considered as (solid) mechanically relevant. Although the model proposed in [67] attempts to incorporate histological information, which is a very promising approach, it is only possible to represent the deformation behavior of axially-symmetric thick-walled vessels. Another drawback is the fact that the artery is considered as a tube reinforced by circularly oriented collagen and elastin fibers, which does not model the real histological situation.

Most of the constitutive models treat the arterial wall as a single layer, but a number of two-layer models have been proposed in the literature. Two-layer models which include anisotropy are those due to, for example, Von Maltzahn et al. [38], Demiray [11] and Rachev [46]. However, the emphasis of the latter paper is on stress-dependent remodeling.

In this section we evaluate and compare some prominent potentials of the exponential, polynomial and logarithmic type which are often used to characterize the overall *passive* behavior of arterial walls. The study aims to illustrate the performance of the potentials and their reliability for the prediction of the state of deformation. In particular, we use a systematic analysis to examine the inflation of a cylindrical tube at various axial stretches λ_z and to compute the evolution of the inner radius r_i with the internal pressure p_i and the reduced axial force F. In addition, at an internal pressure of $p_\mathrm{i} = 13.33$ [kPa] (100 [mm Hg]), the approximate physiological pressure, we evaluate the effect of twist (torsion) on the tube and determine the dependence of the shear γ_i at the inner surface on the torsional couple M_t and the reduced axial force F. However, as will be shown, the mechanical behavior of an anisotropic cylindrical tube under torsion can in general only be investigated if the constitutive model is based on a fully three-dimensional formulation.

4.1. THREE-DIMENSIONAL FORMULATION

This section is concerned with three-dimensional strain-energy functions appropriate for the analysis of *thick-walled* tubes, which is a necessary point of departure for the study of the mechanical behavior of arterial walls.

4.1.1. *Strain-Energy Function Proposed by Delfino et al. [10]*

As already mentioned, the different layers of arterial walls are highly anisotropic due to the organized arrangement of the load carrying (collagen) components. However, there are many *isotropic* strain-energy functions proposed in the literature and used in practice to characterize the mechanical response of arterial walls (see, for example, the oversimplified rubber-like potential used in [30] which cannot represent the strong stiffening effect of arteries in the large strain domain).

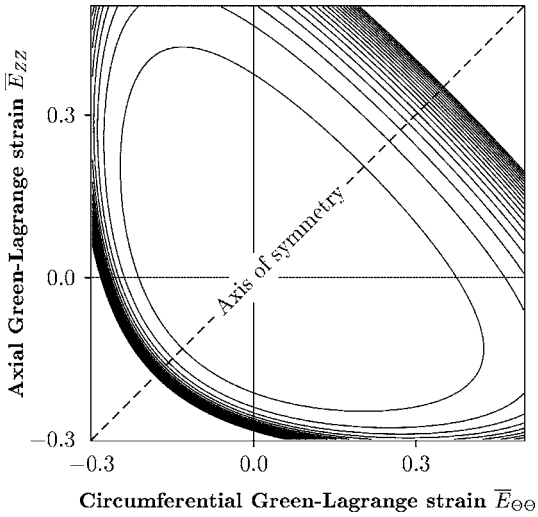

Figure 4. Contour plot of the convex potential (33) with material parameters $a = 44.2$ [kPa] and $b = 16.7$ [–] (see [10]).

Recently, Delfino et al. [10] proposed an (isotropic) rubber-like potential for carotid arteries which is able to model the typical stiffening effects in the high pressure domain. The strain-energy function $\overline{\Psi}$ has the form

$$\overline{\Psi} = \frac{a}{b}\left\{\exp\left[\frac{b}{2}(\bar{I}_1 - 3)\right] - 1\right\} \tag{33}$$

[10], where $a > 0$ is a stress-like material parameter and $b > 0$ is a non-dimensional parameter. The first invariant of the modified right Cauchy–Green tensor $\overline{\mathbf{C}}$ is defined as $\bar{I}_1 = \overline{\mathbf{C}} : \mathbf{I}$. Since the exponential function increases monotonically with $\bar{I}_1$ it is easy to show that strict local convexity of the potential (33) as a function of $\overline{\mathbf{C}}$ (or equivalently $\overline{\mathbf{E}}$) is guaranteed, bearing in mind that because of the incompressibility condition the components of $\overline{\mathbf{E}}$ are not independent.

In the present context, strict local convexity means that the second derivative of Ψ with respect to $\mathbf{E}$ is positive definite, with appropriate modifications to account for incompressibility. This fundamental physical requirement in hyperelasticity ensures that undesirable material instabilities are precluded (for a general discussion of convexity in hyperelasticity the reader is referred to, for example, [42], Section 6, and [7]). It can be shown that strict local convexity of Ψ implies that the contours of constant Ψ are convex, and, in particular, that the projections of these contours in the $(\overline{E}_{\Theta\Theta}, \overline{E}_{ZZ})$-plane are convex. On the other hand, if the contours are not convex then it can be deduced that the potential Ψ is not strictly locally convex. The consequences of this will be seen in the following sections, which show results contrasting with those in Figure 4, in which the (convex) contours are illustrated. For this figure we have used material parameters $a = 44.2$ [kPa] and $b = 16.7$ [–]

Table I. Material and geometrical data of a human carotid artery [10].

Material	Geometry	
$a = 44.2$ [kPa]	$\alpha = 0.0°$	$\alpha = 100.0°$
$b = 16.7$ [–]	$R_\mathrm{i} = 3.1$ [mm]	$R_\mathrm{i} = 4.46$ [mm]
	$R_\mathrm{o} = 4.0$ [mm]	$R_\mathrm{o} = 5.36$ [mm]

as proposed in [10]. Since the potential is isotropic the contour plots are symmetric in the line which bisects the axes.

For the function (33) the isochoric contribution $\overline{\boldsymbol{\sigma}}$ to the Cauchy stress tensor $\boldsymbol{\sigma}$ is obtained from $(10)_3$ as

$$\overline{\boldsymbol{\sigma}} = 2\overline{\Psi}_1 \operatorname{dev} \overline{\mathbf{b}}, \tag{34}$$

where $\overline{\Psi}_1 = \partial\overline{\Psi}/\partial\bar{I}_1$ and $\overline{\mathbf{b}}$ is the modified left Cauchy–Green tensor. Note that $J = 1$.

Hence, with the definition (3) of the left Cauchy–Green tensor, the isochoric Cauchy stress components, which are used in equations $(27)_1$, $(27)_2$ and (29), are given by (34). In order to investigate the specific arterial response we use the material constants for a human carotid artery given in [10]. The values are given in Table I. For the description of the stress-free configuration we have taken $\alpha = 100.0°$, which is based on the value in [10] adjusted for the different definitions of opening angle. For consistency we take the geometry in the unloaded configuration for the residually stressed case to be the same as that for the case without residual stress. The geometry in the unstressed configuration is obtained using the incompressibility condition, which furnishes a connection between the inner and outer radii in this configuration, together with the simplifying assumption of unchanged wall thickness. The resulting values are given in Table I. In addition, for purposes of comparison of the shear γ_i at the inner surface of the tube, the undeformed length L of the arterial tube was taken to be equal to the value of the inner radius R_i corresponding to $\alpha = 0.0°$. This was followed for all the cylinder models studied subsequently.

This basis for the computation of the radii in the stress-free configuration is also adopted in the following sections. The values of the material constants that we use for our investigations are those given in the papers in which the energy functions were introduced. We note that these values were determined under the assumption that the unloaded configuration is stress free (it is not clear if the same assumption was used in [10]).

The *in vivo* axial pre-stretch is based on *in situ* measurements prior to removal of the artery and is given as $\lambda_z = 1.1$ (see [10]). The mechanical response of the human carotid artery during inflation and torsion is shown in Figure 5. The internal

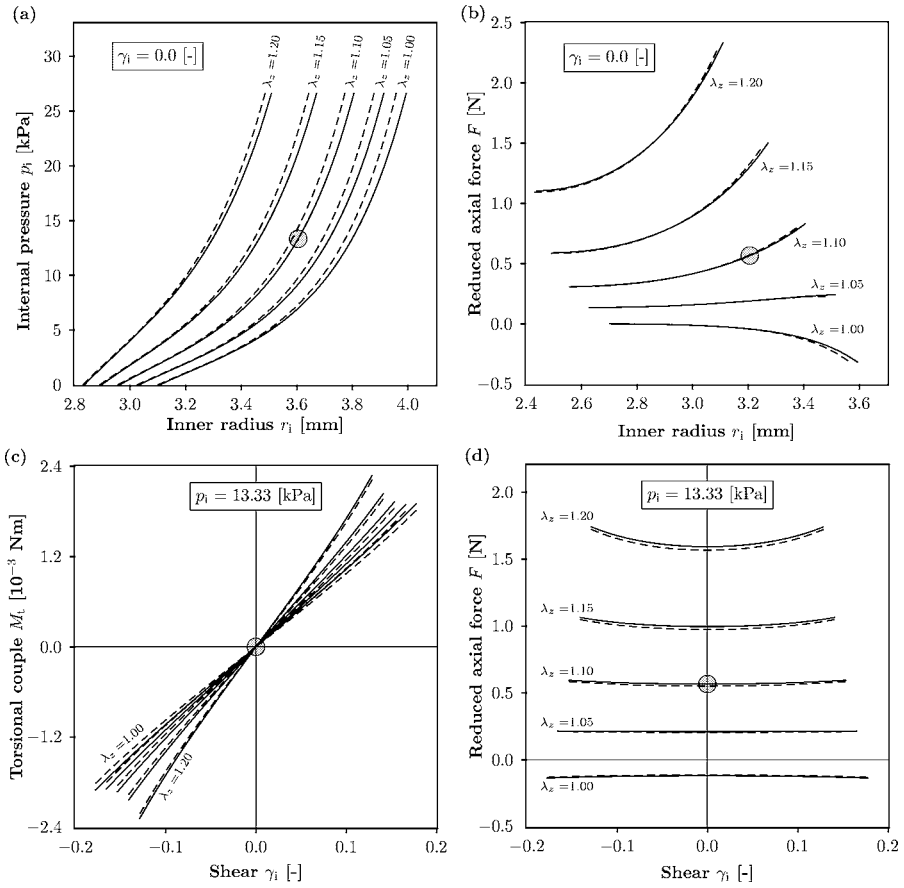

Figure 5. Deformation behavior of a human carotid artery during inflation and torsion using the constitutive model proposed in [10]. Solid lines are numerical results with residual strains included ($\alpha = 100.0°$) while the dashed lines are results without residual strains ($\alpha = 0.0°$). Dependence of (a) the internal pressure p_i and (b) the reduced axial force F on the inner radius r_i in the absence of shear deformation ($\gamma_i = 0$). Dependence of (c) the torsional couple M_t and (d) the reduced axial force F on the shear γ_i at fixed internal pressure $p_i = 13.33$ [kPa]. The shaded circles indicate the approximate central region of the physiological state.

pressure p_i and the angle of twist Φ are varied within the ranges

$$0 \leqslant p_i \leqslant 26.67 \text{ [kPa]} \quad \text{and} \quad -0.15 \leqslant \Phi \leqslant 0.15 \text{ [rad]}. \tag{35}$$

These loadings are applied at fixed axial stretches of the artery varying between $\lambda_z = 1.0$ and $\lambda_z = 1.2$.

The predicted response is in good qualitative agreement with the experimentally observed mechanical behavior of arteries; see, for example, the survey article [32] or compare with the (rare) data on shear tests of arteries provided in [12]. With the potential (33) the typical stiffening effect at high pressures can be replicated, as can be seen in Figure 5(a). Remarkably, the reduced axial force F is hardly

influenced by the changes of internal pressures p_i at $\lambda_z = 1.05$, which is close to the physiological pre-stretch of $\lambda_z = 1.1$; see Figure 5(b). In Figure 5(c) and (d) respectively the torsional couple M_t and the reduced axial force F are plotted against the amount of shear at the inner surface, i.e. $\gamma_\mathrm{i} = \Phi r_\mathrm{i}/l = \Phi r_\mathrm{i}/\lambda_z L$.

The solid lines show numerical results based on a load-free, but not stress-free, configuration ($\alpha = 100.0°$), while the dashed lines are based on a load-free and stress-free configuration ($\alpha = 0.0°$). As illustrated in Figure 5(a), residual stresses influence the internal pressure/inner radius behavior moderately, while Figure 5(b)–(d) shows a very minor influence of the residual stresses on the global mechanical response of the artery. Note that incorporation of the residual stresses in the load-free configuration softens the material of the artery in the sense that a given inner radius r_i is achieved with a lower internal pressure p_i, a finding which is in agreement with the analytical studies of Humphrey [32], p. 101.

4.1.2. *Strain-Energy Function of Fung's Type*

The strain-energy function used most extensively for arteries appears to be the two-dimensional exponential form proposed by Fung et al. [18]. A generalization to the three-dimensional regime, presented by Chuong and Fung [5], assumes that the principal directions of the stress tensor coincide with the radial, circumferential and axial directions of the artery. Shear deformations due to, for example, torsion of the artery, were not considered. To incorporate shear deformations $\overline{E}_{\Theta Z}$ in the shear planes $z =$ constant, Deng et al. [12] proposed an extension of the classical two-dimensional function given in [18].

Many modifications of these strain-energy functions have been published subsequently. For example, a combined polynomial-exponential form of the strain-energy function incorporating shear deformations was given by Kas'yanov and Rachev [35]. The most general strain-energy function of *Fung's* type is formulated by Humphrey [32]. It is suitable for arbitrary (three-dimensional) states of deformations and has the form

$$\overline{\Psi} = \frac{1}{2}c[\exp(Q) - 1], \tag{36}$$

where c is a material parameter and Q is given by

$$\begin{aligned} Q \;=\; & b_1\overline{E}^2_{\Theta\Theta} + b_2\overline{E}^2_{ZZ} + b_3\overline{E}^2_{RR} + 2b_4\overline{E}_{\Theta\Theta}\overline{E}_{ZZ} + 2b_5\overline{E}_{ZZ}\overline{E}_{RR} \\ & + 2b_6\overline{E}_{RR}\overline{E}_{\Theta\Theta} + b_7\overline{E}^2_{\Theta Z} + b_8\overline{E}^2_{RZ} + b_9\overline{E}^2_{R\Theta}. \end{aligned} \tag{37}$$

Here b_i, $i = 1, \ldots, 9$, are non-dimensional material parameters, while $\overline{E}_{IJ}$, for $I, J = R, \Theta, Z$, are the components of the modified Green–Lagrange strain tensor referred to cylindrical polar coordinates (R, Θ, Z).

In the work of Fung et al. [18] and Chuong and Fung [5] there is no *a priori* restriction on the material parameters presented. However, it is important to note that in order for the (anisotropic) function $\overline{\Psi}$ to be convex in the sense discussed

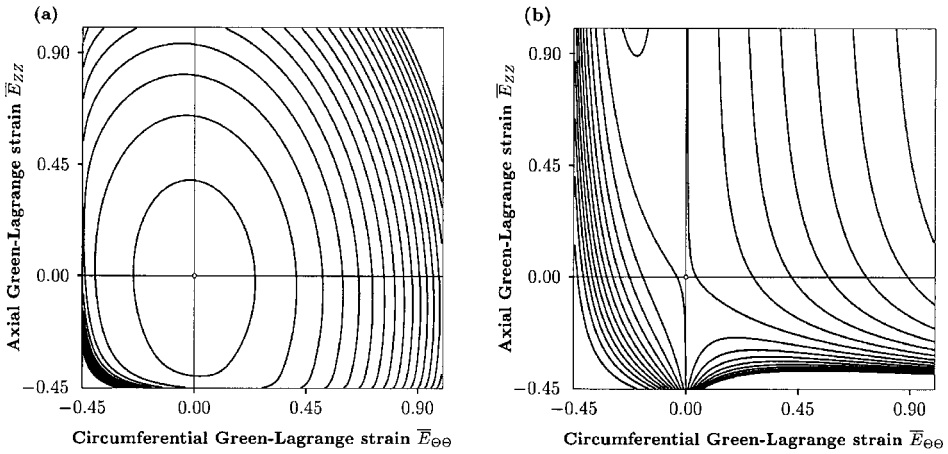

Figure 6. Contour plots of the potential (36) with (a) material parameters c, $b_1, \ldots, b_7$ in Table II, and (b) a set of parameters chosen to illustrate non-convexity.

Table II. Material and geometrical data for a rabbit carotid artery in respect of (37) (see experiment 71 in [5]; b_7 is based on the study in [12]).

Material	Geometry	
$c = 26.95$ [kPa]	$\alpha = 0.0°$	$\alpha = 160.0°$
$b_1 = 0.9925$ [–]		
$b_2 = 0.4180$ [–]	$R_\mathrm{i} = 0.71$ [mm]	$R_\mathrm{i} = 1.43$ [mm]
$b_3 = 0.0089$ [–]	$R_\mathrm{o} = 1.10$ [mm]	$R_\mathrm{o} = 1.82$ [mm]
$b_4 = 0.0749$ [–]		
$b_5 = 0.0295$ [–]		
$b_6 = 0.0193$ [–]		
$b_7 = 5.0000$ [–]		

in Section 4.1.1 the material parameters $b_1, \ldots, b_9$ must not be chosen arbitrarily. Figure 6(a) shows a contour plot of the potential (36) with the material parameters proposed in [5] (see the summary in Table II), while the contour plot in Figure 6(b) uses an alternative set of parameters chosen to illustrate non-convexity of the strain-energy function. This is one of many possible choices which lead to non-convexity. The 'physical' meanings of the individual parameters are unclear (see the discussion in the book by Fung [17], Section 8.6.2). Hence, if this strain-energy function is used care must be taken to select appropriate restrictions on the values of c and b_i, since unconstrained parameter optimization does not, in general, guarantee convexity. It is therefore important to be sure that the optimization process is performed within a range of parameters for which convexity is assured.

Furthermore, in the computational context, in order to obtain solutions of complex nonlinear (initial boundary-value) problems, incremental/iterative solution techniques of Newton's type are frequently applied to solve a sequence of linearized problems. These techniques, often employed in computational biomechanics, use predicted states of deformation which might be far from the range of deformation for which the experimental tests were conducted. This might lead to numerical problems within the solution procedure when strain-energy functions are used which are not convex *a priori*. To be specific, parameters used outside the range for which the fitting process was performed might induce a non-convex potential. A further comment on parameter identification for the strain-energy function (36) used in combination with relation (37) is appropriate. Because of the large number of material parameters b_i a least-square procedure can lead to problems of non-uniqueness associated with their sensitivity to small changes in the data, as pointed out, for example, by Fung [17], Section 8.6.1.

With equations (36) and $(10)_3$ the components of the isochoric part of the Cauchy stress tensor may be obtained in the cylindrical polar coordinate system (r, θ, z), so that it is a straightforward task to solve the equilibrium equation $(27)_1$ and to calculate the torsional couple M_t and the reduced axial force F, as given by equations $(27)_2$ and (29), respectively. The material and geometrical data used for this computation are from a carotid artery of a rabbit and are summarized in Table II. The values of the parameters c and b_i, $i = 1, \ldots, 6$, are taken from [5], while b_7 is an estimated value (measuring the resistance to distortion) based on the shear moduli of arteries as presented in [12]. Since the associated shear strains $\overline{E}_{ZR}$ and $\overline{E}_{R\Theta}$ vanish in the considered problem, the parameters b_8 and b_9 need not be considered. In order to investigate the influence of residual stresses on the global response of the artery, two different stress-free states are considered, namely $\alpha = 0.0°$ and $\alpha = 160.0°$. The (mean) value 160.0° is based on the study [23].

The *in vivo* axial pre-stretch of the artery is given as $\lambda_z = 1.695$ (calculated from the axial component of the Green–Lagrange strain given in [18], Table I, experiment 71) and the internal pressure p_i and the angle of twist Φ are varied within the ranges

$$0 \leqslant p_i \leqslant 21.33 \text{ [kPa]} \quad \text{and} \quad -0.10 \leqslant \Phi \leqslant 0.10 \text{ [rad]} \tag{38}$$

(compare with [12, 18]). These loads are applied at fixed axial stretches of the artery varying between $\lambda_z = 1.5$ and $\lambda_z = 1.9$. Figure 7 shows the computed deformation behavior of the artery under various loading conditions. The influence of residual strain on the deformation field is much larger than was the case in the study of Section 4.1.1 (see Figure 5). This is because the opening angle α and the ratio of the wall thickness to the diameter were larger than the values used in Section 4.1.1. Note that at $\lambda_z = 1.9$ the reduced axial force F first increases with the inner radius r_i and then, at high pressures, it tends to decrease; see Figure 7(b). This characteristic is not observed experimentally.

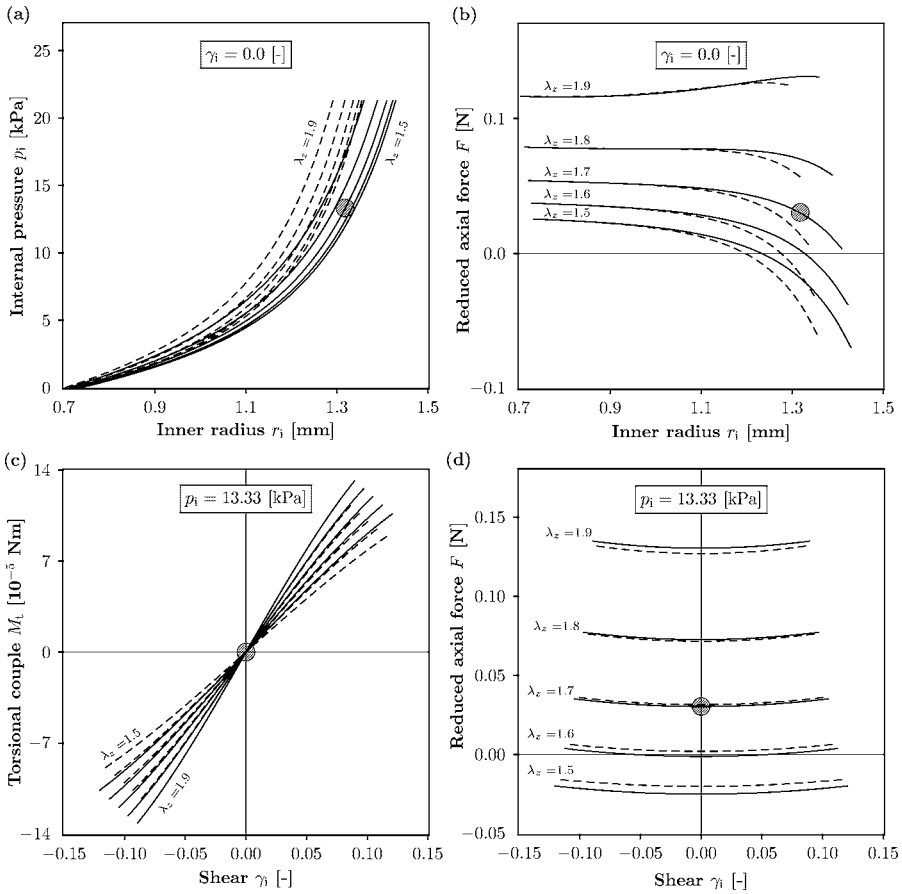

Figure 7. Deformation behavior of a rabbit carotid artery during inflation and torsion for the constitutive model (36), (37) with $b_8 = b_9 = 0$. Solid lines are numerical data with residual strains included ($\alpha = 160.0°$) while the dashed lines are results without residual strains ($\alpha = 0.0°$). Dependence of (a) the internal pressure p_i and (b) the reduced axial force F on inner radius r_i without shear deformation ($\gamma_i = 0$). Dependence of (c) the torsional couple M_t and (d) the reduced axial force F on the shear γ_i at fixed internal pressure $p_i = 13.33$ [kPa]. The shaded circles indicate the approximate central region of the physiological state.

4.2. TWO-DIMENSIONAL FORMULATION

Since it is generally accepted that it is appropriate to treat arterial walls as incompressible materials, the restriction $J = 1$ can be used to find alternative expressions for the strain-energy function $\overline{\Psi}$, which, in general, is a function of the strain components $\overline{E}_{RR}$, $\overline{E}_{\Theta\Theta}$, $\overline{E}_{ZZ}$, $\overline{E}_{R\Theta}$, $\overline{E}_{RZ}$, $\overline{E}_{\Theta Z}$. The alternative potential $\hat{\overline{\Psi}}(\overline{E}_{\Theta\Theta}, \overline{E}_{ZZ}, \overline{E}_{\Theta Z})$, which we refer to as the *two-dimensional* counterpart of $\overline{\Psi}$, is very popular and used frequently in the literature. Such a two-dimensional formulation is not capable of describing the three-dimensional *anisotropic* behavior of a thick-walled cylindrical tube under, for example, inflation and torsion. However,

for the special case of combined bending, inflation and axial extension the potential $\overline{\hat{\Psi}}$ is suitable for predicting the three-dimensional state of stress. A comparative study of three important examples of such potentials concludes this section.

4.2.1. *The Strain-Energy Function* $\overline{\hat{\Psi}}(\overline{E}_{\Theta\Theta}, \overline{E}_{ZZ}, \overline{E}_{\Theta Z})$

We consider a thick-walled cylindrical tube of incompressible material deformed in such a way that the modified Green–Lagrange strains $\overline{E}_{R\Theta}$ and $\overline{E}_{RZ}$ are zero, as is the case for the deformation considered in Section 3.2. Using these assumptions and with elimination of $\overline{E}_{RR}$ via the incompressibility constraint an alternative two-dimensional approximation of $\overline{\Psi}$ may be given in the form

$$\overline{\Psi}(\overline{E}_{RR}, \overline{E}_{\Theta\Theta}, \overline{E}_{ZZ}, \overline{E}_{R\Theta}, \overline{E}_{RZ}, \overline{E}_{\Theta Z}) = \overline{\hat{\Psi}}(\overline{E}_{\Theta\Theta}, \overline{E}_{ZZ}, \overline{E}_{\Theta Z}), \tag{39}$$

where $\overline{\hat{\Psi}}$ is a strain energy with the three independent strain variables $\overline{E}_{\Theta\Theta}$, $\overline{E}_{ZZ}$, $\overline{E}_{\Theta Z}$. Using the chain rule, the derivatives

$$\frac{\partial \overline{\hat{\Psi}}}{\partial \overline{E}_{\alpha}} = \frac{\partial \overline{\Psi}}{\partial \overline{E}_{\alpha}} + \frac{\partial \overline{\Psi}}{\partial \overline{E}_{RR}} \frac{\partial \overline{E}_{RR}}{\partial \overline{E}_{\alpha}}, \quad \alpha = \Theta\Theta, ZZ, \Theta Z, \tag{40}$$

are obtained. The constraint $\det \overline{\mathbf{C}} = \det(2\overline{\mathbf{E}} + \mathbf{I}) = 1$ and equation $(20)_2$ enable $\overline{E}_{RR}$ to be expressed in terms of the independent components $\overline{E}_{\Theta\Theta}$, $\overline{E}_{ZZ}$, $\overline{E}_{\Theta Z}$ according to

$$\overline{E}_{RR} = \frac{1}{2}\big\{[(2\overline{E}_{\Theta\Theta} + 1)(2\overline{E}_{ZZ} + 1) - 4\overline{E}_{\Theta Z}^2]^{-1} - 1\big\}. \tag{41}$$

Hence, with (41), we find from (40) that

$$\frac{\partial \overline{\Psi}}{\partial \overline{E}_{\Theta\Theta}} = \frac{\partial \overline{\hat{\Psi}}}{\partial \overline{E}_{\Theta\Theta}} + (2\overline{E}_{ZZ} + 1)(2\overline{E}_{RR} + 1)^2 \frac{\partial \overline{\Psi}}{\partial \overline{E}_{RR}}, \tag{42}$$

$$\frac{\partial \overline{\Psi}}{\partial \overline{E}_{ZZ}} = \frac{\partial \overline{\hat{\Psi}}}{\partial \overline{E}_{ZZ}} + (2\overline{E}_{\Theta\Theta} + 1)(2\overline{E}_{RR} + 1)^2 \frac{\partial \overline{\Psi}}{\partial \overline{E}_{RR}}, \tag{43}$$

$$\frac{\partial \overline{\Psi}}{\partial \overline{E}_{\Theta Z}} = \frac{\partial \overline{\hat{\Psi}}}{\partial \overline{E}_{\Theta Z}} - 4\overline{E}_{\Theta Z}(2\overline{E}_{RR} + 1)^2 \frac{\partial \overline{\Psi}}{\partial \overline{E}_{RR}}. \tag{44}$$

The aim now is to solve the equilibrium equation $(27)_1$, which requires the stress difference $\overline{\sigma}_{\theta\theta} - \overline{\sigma}_{rr}$. From the stress equation $(10)_3$ and the kinematic relation $(19)_2$ we find that $\overline{\sigma}_{\theta\theta} = \lambda_\theta^2 \partial\overline{\Psi}/\partial\overline{E}_{\Theta\Theta} + 2\gamma\lambda_z\lambda_\theta \partial\overline{\Psi}/\partial\overline{E}_{\Theta Z} + \gamma^2\lambda_z^2 \partial\overline{\Psi}/\partial\overline{E}_{ZZ}$ and $\overline{\sigma}_{rr} = \lambda_r^2 \partial\overline{\Psi}/\partial\overline{E}_{RR}$. Using equations (42)–(44) we find that the stress difference cannot be given in terms of the potential $\overline{\hat{\Psi}}$ alone since the expression $\partial\overline{\Psi}/\partial\overline{E}_{RR}$ cannot in general be eliminated and remains undetermined. Moreover, $\overline{\sigma}_{\theta z}$ similarly depends on $\partial\overline{\Psi}/\partial\overline{E}_{RR}$. This means, in particular, that it is not in general possible to use

the alternative potential $\hat{\overline{\Psi}}$ to derive the complete state of stress in an anisotropic cylindrical tube under inflation and torsion in a three-dimensional context.

It is worth noting, however, that the particular stress combinations

$$\overline{\sigma}_{\theta\theta} - \overline{\sigma}_{rr} - 2\gamma\overline{\sigma}_{\theta z} = \lambda_\theta^2 \frac{\partial \hat{\overline{\Psi}}}{\partial \overline{E}_{\Theta\Theta}} - \gamma^2\lambda_z^2 \frac{\partial \hat{\overline{\Psi}}}{\partial \overline{E}_{ZZ}}, \tag{45}$$

$$\overline{\sigma}_{zz} - \overline{\sigma}_{rr} = \lambda_z^2 \frac{\partial \hat{\overline{\Psi}}}{\partial \overline{E}_{ZZ}} \tag{46}$$

are given in terms of $\hat{\overline{\Psi}}$, and we note that $\lambda_\theta^2 = 2\overline{E}_{\Theta\Theta} + 1$, $(1+\gamma^2)\lambda_z^2 = 2\overline{E}_{ZZ} + 1$.

Exceptionally, for an isotropic material, since the Cauchy stress tensor is coaxial with the left Cauchy–Green tensor, the universal relation

$$\gamma\lambda_z^2(\overline{\sigma}_{\theta\theta} - \overline{\sigma}_{zz}) = (\lambda_\theta^2 + \gamma^2\lambda_z^2 - \lambda_z^2)\overline{\sigma}_{\theta z} \tag{47}$$

is obtained. This can be shown as follows. Let $\cos\phi\mathbf{e}_\theta + \sin\phi\mathbf{e}_z$ denote a principal axis of the Cauchy–Green tensor $\mathbf{b}$. Then, using (21), the angle ϕ may be calculated in the form

$$\tan 2\phi = \frac{2\gamma\lambda_z^2}{\lambda_\theta^2 + \gamma^2\lambda_z^2 - \lambda_z^2}, \tag{48}$$

while, for the Cauchy stresses, we have

$$\tan 2\phi = \frac{2\overline{\sigma}_{\theta z}}{\overline{\sigma}_{\theta\theta} - \overline{\sigma}_{zz}}. \tag{49}$$

The combination of (45)–(47) enables the normal stress differences and the shear stress to be expressed in terms of $\hat{\overline{\Psi}}$. We omit the details since consideration of isotropic models is not of interest here.

REMARK 4.1. For an anisotropic material, in the special case $\gamma = 0$ (no shear deformation), equations $(27)_1$ and (28) can be solved on the basis of the two-dimensional form of strain-energy function $\hat{\overline{\Psi}}(\overline{E}_{\Theta\Theta}, \overline{E}_{ZZ}, \overline{E}_{\Theta Z})$. With $\gamma = 0$, it follows from (45) that

$$\overline{\sigma}_{\theta\theta} - \overline{\sigma}_{rr} = (1 + 2\overline{E}_{\Theta\Theta}) \frac{\partial \hat{\overline{\Psi}}}{\partial \overline{E}_{\Theta\Theta}}. \tag{50}$$

Using (46) together with (50) the expression $2\overline{\sigma}_{zz} - \overline{\sigma}_{\theta\theta} - \overline{\sigma}_{rr}$ in (29) is then obtained in the form

$$2\overline{\sigma}_{zz} - \overline{\sigma}_{\theta\theta} - \overline{\sigma}_{rr} = 2(1 + 2\overline{E}_{ZZ}) \frac{\partial \hat{\overline{\Psi}}}{\partial \overline{E}_{ZZ}} - (1 + 2\overline{E}_{\Theta\Theta}) \frac{\partial \hat{\overline{\Psi}}}{\partial \overline{E}_{\Theta\Theta}}. \tag{51}$$

Hence, the reduced axial force F may be expressed in terms of the strain energy $\hat{\overline{\Psi}}$.

Table III. Material and geometrical data for a rabbit carotid artery based on the potential (52) (see experiment 71 in [18]).

Material	Geometry	
$c_1 = -24.385$ [kPa]	$\alpha = 0.0°$	$\alpha = 160.0°$
$c_2 = -3.589$ [kPa]		
$c_3 = -1.982$ [kPa]	$R_\mathrm{i} = 0.71$ [mm]	$R_\mathrm{i} = 1.43$ [mm]
$c_4 = 46.334$ [kPa]	$R_\mathrm{o} = 1.10$ [mm]	$R_\mathrm{o} = 1.82$ [mm]
$c_5 = 32.321$ [kPa]		
$c_6 = 3.743$ [kPa]		
$c_7 = 3.266$ [kPa]		

4.2.2. *Strain-Energy Function Proposed by Vaishnav et al. [62]*

Two-dimensional forms of strain-energy functions suitable for the description of the deformation behavior of canine thoracic aorta using polynomial expressions have been proposed by Vaishnav et al. [62]. This classic paper presents three polynomial expressions with 3, 7 or 12 material parameters. As studied in [62] the three-parameter model is too inaccurate for a serious investigation and the twelve-parameter model does not have a significant advantage over the seven-parameter model. Hence, in the present paper we focus attention on the seven-parameter model, which is written in the form

$$\begin{aligned}\hat{\overline{\Psi}} \;=\; & c_1\overline{E}^2_{\Theta\Theta} + c_2\overline{E}_{\Theta\Theta}\overline{E}_{ZZ} + c_3\overline{E}^2_{ZZ} + c_4\overline{E}^3_{\Theta\Theta} + c_5\overline{E}^2_{\Theta\Theta}\overline{E}_{ZZ} \\ & + c_6\overline{E}_{\Theta\Theta}\overline{E}^2_{ZZ} + c_7\overline{E}^3_{ZZ},\end{aligned} \tag{52}$$

where $c_1, \ldots, c_7$ are stress-like material parameters and $\overline{E}_{\Theta\Theta}$ and $\overline{E}_{ZZ}$ are the components of the modified Green–Lagrange strain tensor in the circumferential and axial directions, respectively. In Fung et al. [18] the form (52) was used to fit the parameters $c_1, \ldots, c_7$ to experimental data from rabbit carotid arteries. The result is summarized in Table III. Note that with these values of the material parameters the strain-energy function (52) is not convex, as the contour plot in Figure 8 shows. In fact, because of the cubic nature of the strain-energy function (52), it is not convex for *any* set of values of the material constants.

While the performance of the constitutive law (52) is acceptable in the tensile region ($\overline{E}_{\Theta\Theta} > 0$, $\overline{E}_{ZZ} > 0$), it fails for compressive strains. Moreover, Fung [17] showed that two completely different sets of material parameters $c_1, \ldots, c_7$ are able to represent the mechanical response of the same artery quite well. This lack of uniqueness of the material parameters is problematic. Note that a polynomial expression, different from that in [62], has been proposed in [63] in order to model the *three-dimensional* anisotropic behavior of a canine carotid artery and of a rabbit aorta.

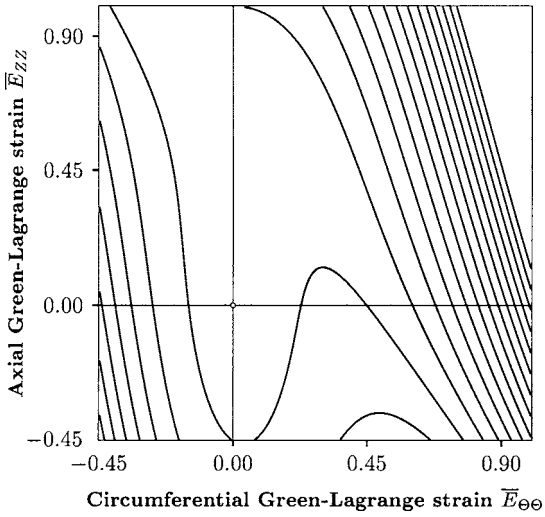

Figure 8. Contour plot of the potential (52) with material parameters given in Table III.

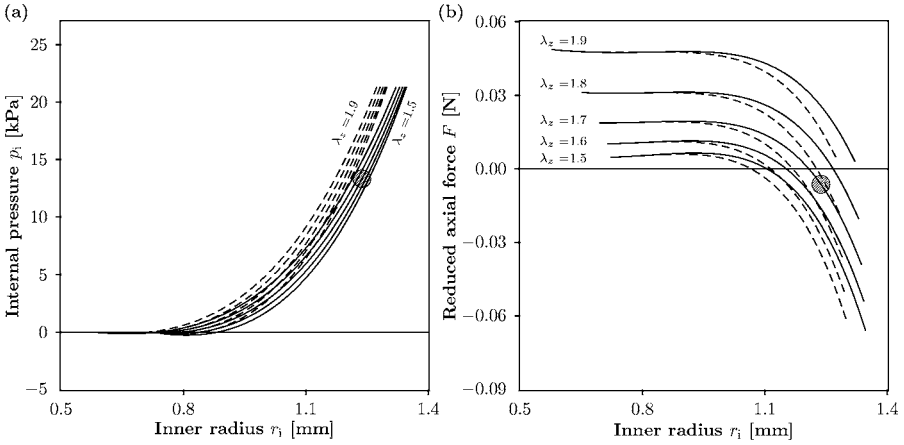

Figure 9. Deformation behavior of a rabbit carotid artery during inflation based on the constitutive model in [62]. Solid lines are numerical results with residual strains included ($\alpha = 160.0°$) while dashed lines are results without residual strains ($\alpha = 0.0°$). Dependence of (a) the internal pressure p_i, and (b) the reduced axial force F on the inner radius r_i, without shear deformation ($\gamma_i = 0$). The shaded circles indicate the approximate central region of the physiological state.

Using (52) we may solve the equilibrium equation $(27)_1$ and calculate the reduced axial force F from equation (29). For this purpose, we use the formulas (50) and (51) and apply the procedure described in Remark 3.2. The material and geometrical data for a rabbit carotid artery are as summarized in Table III and we use the same set of geometrical data and the same range of loading as in Section 4.1.2.

Figure 9 shows the predicted mechanical response of the considered artery (experiment 71 in [18]). The dependence of the internal pressure p_i on the inner radius

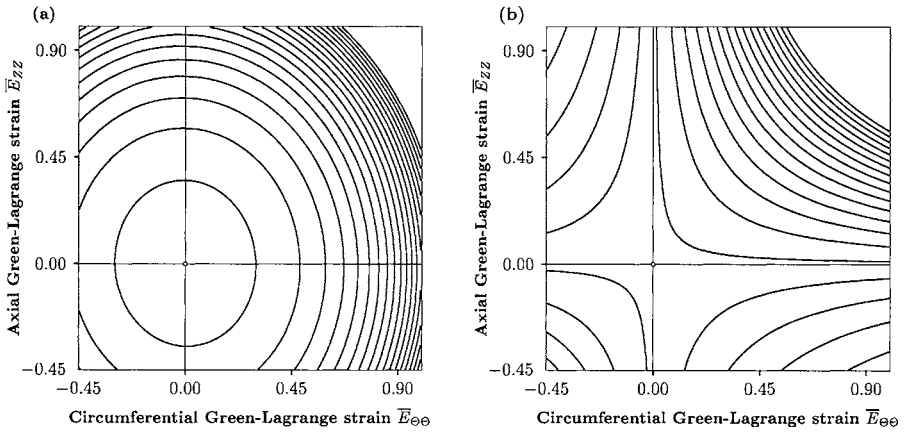

Figure 10. Contour plots of the potential (53) with (a) material parameters given in Table IV, adopted from [59], and (b) with a set of parameters chosen to illustrate non-convexity.

r_{i} is plotted in Figure 9(a). Note that the solution of the equilibrium equation $(27)_1$ is not unique, since, for example, $p_{\mathrm{i}} = 0$ corresponds to two different values of r_{i}. This is a consequence of the non-convexity of the potential. The dependence of the reduced axial force F on the inner radius r_{i} is plotted in Figure 9(b). As can be seen, for axial stretches higher than the typical physiological stretch, the characteristic increase of F with the inner radius r_{i} illustrated in Figures 5(b) and 7(b) is not predicted by the potential (52) with the set of material parameters given in Table III.

The potential (52) represents the first attempt to describe the *anisotropic* mechanical response of arteries. However, as indicated above, its applicability is limited.

4.2.3. *Strain-Energy Function Proposed by Fung et al. [18]*

The well-known exponential strain-energy function due to Fung et al. [18] has been proposed in the two-dimensional form

$$\hat{\overline{\Psi}} = \frac{1}{2}c[\exp(\hat{Q}) - 1], \quad \hat{Q} = b_1\overline{E}^2_{\Theta\Theta} + b_2\overline{E}^2_{ZZ} + 2b_4\overline{E}_{\Theta\Theta}\overline{E}_{ZZ}, \tag{53}$$

where c is a stress-like material parameter and b_1, b_2, b_4 are non-dimensional parameters. However, as discussed in Section 4.1.2, the material parameters cannot be chosen arbitrarily if convexity of the function (53) is desired. Contour plots of the potential (53) are shown in Figure 10. The material parameters proposed in [59], and given in Table IV, are used in Figure 10(a), in which case the contours are convex. On the other hand, non-convexity is illustrated in Figure 10(b) in respect of a specific choice of parameters. As in the case of Section 4.1.2, the non-convexity can be demonstrated for a wide range of parameter values. This is easy to check because of the quadratic nature of $\hat{Q}$ in equation $(53)_2$. In fact, it can be shown, for example, that if $c > 0$, then (53) is strictly locally convex *if and only if* $b_1 > 0$, $b_2 > 0$ and $b_1 b_2 > b_4^2$.

Table IV. Material and geometrical data for a dog carotid artery based on the potential (53) (see experiment D850815C in [59]).

Material	Geometry	
$c = 28.58$ [kPa]	$\alpha = 0.0°$	$\alpha = 160.0°$
$b_1 = 0.8329$ [–]		
$b_2 = 0.6004$ [–]	$R_\mathrm{i} = 1.21$ [mm]	$R_\mathrm{i} = 2.40$ [mm]
$b_4 = 0.0169$ [–]	$R_\mathrm{o} = 1.77$ [mm]	$R_\mathrm{o} = 2.96$ [mm]

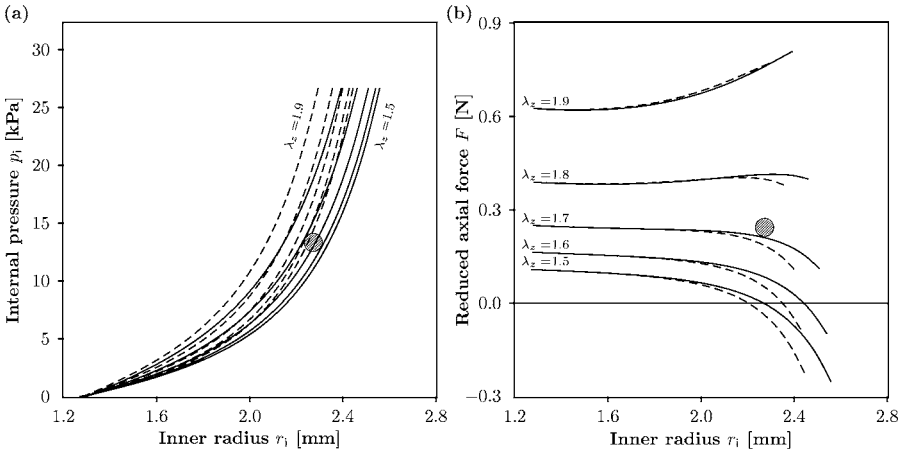

Figure 11. Deformation behavior of a dog carotid artery (see experiment D850815C in [59]) during inflation using the constitutive model in [18]. Solid lines are numerical results with residual strains included ($\alpha = 160.0°$) while the dashed lines are results without residual strains ($\alpha = 0.0°$). Dependence of (a) the internal pressure p_i and (b) the reduced axial force F on the inner radius r_i, without shear deformation ($\gamma_\mathrm{i} = 0$). The shaded circles indicate the approximate central region of the physiological state.

By means of equations (53) and (50) we may solve the equation of equilibrium $(27)_1$ and calculate the reduced axial force F, as outlined in Remark 3.2. The resulting response is shown in Figure 11 for the material and geometrical data given in Table IV. In order to investigate the influence of residual stresses on the response of the artery, two different stress-free states are considered ($\alpha = 0.0°$ and $\alpha = 160.0°$). The *in vivo* axial pre-stretch of the artery is given as $\lambda_z = 1.72$ and the internal pressure p_i is varied within the range

$$0 \leqslant p_\mathrm{i} \leqslant 26.67 \text{ [kPa]} \tag{54}$$

(see experiment D850815C in [59]). The inflation is considered at fixed axial stretches of the artery between $\lambda_z = 1.5$ and $\lambda_z = 1.9$.

The potential (53) is able to model the basic characteristics of the mechanical behavior of arteries except in the low pressure domain. The problem in the low

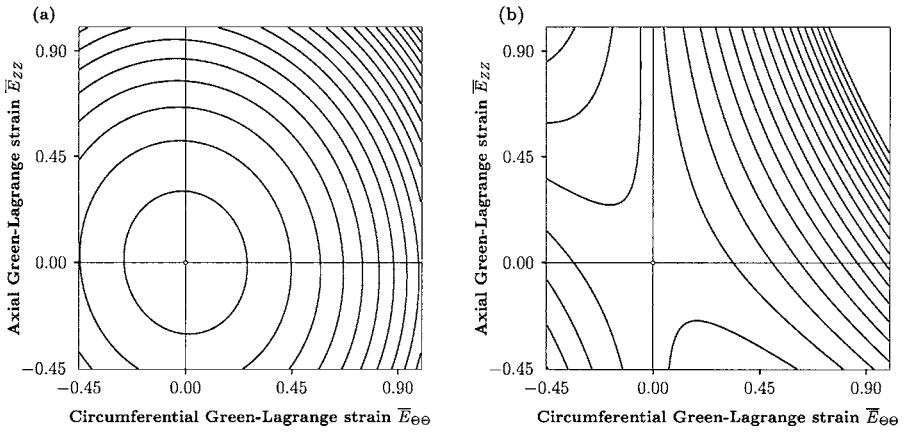

Figure 12. Contour plots of the potential (55) with (a) material parameters given in Table V, adopted from [59], and (b) a set of parameters chosen to illustrate non-convexity.

pressure domain, as can be seen in Figure 11(a), is that r_{i} is independent of the axial stretch when $p_{\mathrm{i}} = 0$. A strong influence of the residual stresses on the $p_{\mathrm{i}} - r_{\mathrm{i}}$ behavior is observed.

4.2.4. *Strain-Energy Function Proposed by Takamizawa and Hayashi [59]*

Another well-known two-dimensional form of strain-energy function for arteries was proposed by Takamizawa and Hayashi [59]. It has the logarithmic form

$$\hat{\overline{\Psi}} = -c\mathrm{Ln}(1 - \psi), \tag{55}$$

where c is a stress-like material parameter and the function ψ is given in the form

$$\psi = \frac{1}{2}b_1\overline{E}^2_{\Theta\Theta} + \frac{1}{2}b_2\overline{E}^2_{ZZ} + b_4\overline{E}_{\Theta\Theta}\overline{E}_{ZZ}. \tag{56}$$

Here b_1, b_2, b_4 are non-dimensional material parameters and $\overline{E}_{\Theta\Theta}$, $\overline{E}_{ZZ}$ are the components of the modified Green–Lagrange strain tensor $\overline{\mathbf{E}}$ in the circumferential and axial directions, respectively.

Note that the proposed definition (56) does not, in general, preclude ψ from being 1, which leads to an infinite value of $\hat{\overline{\Psi}}$ in certain states of deformation. Furthermore, for $\psi > 1$, the argument of the logarithmic function (55) is negative and the function is not then defined. This type of strain-energy function is therefore only applicable for a limited range of states of deformation. Moreover, it is convex under the same conditions as discussed in respect to (53). The material parameters proposed in [59], and given in Table V, are used to produce the convex contours in Figure 12(a), while an alternative set of parameters is used in Figure 12(b) to illustrate non-convexity of the strain-energy function.

Using equations (55), (56) and (50) we may solve equation $(27)_1$ and calculate the reduced axial force F, as outlined in Remark 3.2. The material data for

Table V. Material and geometrical data for a dog carotid artery based on (55) (see experiment D850815C in [59]).

Material	Geometry	
$c = 57.94$ [kPa]	$\alpha = 0.0°$	$\alpha = 160.0°$
$b_1 = 0.6311$ [–]		
$b_2 = 0.4728$ [–]	$R_\mathrm{i} = 1.21$ [mm]	$R_\mathrm{i} = 2.40$ [mm]
$b_4 = 0.0301$ [–]	$R_\mathrm{o} = 1.77$ [mm]	$R_\mathrm{o} = 2.96$ [mm]

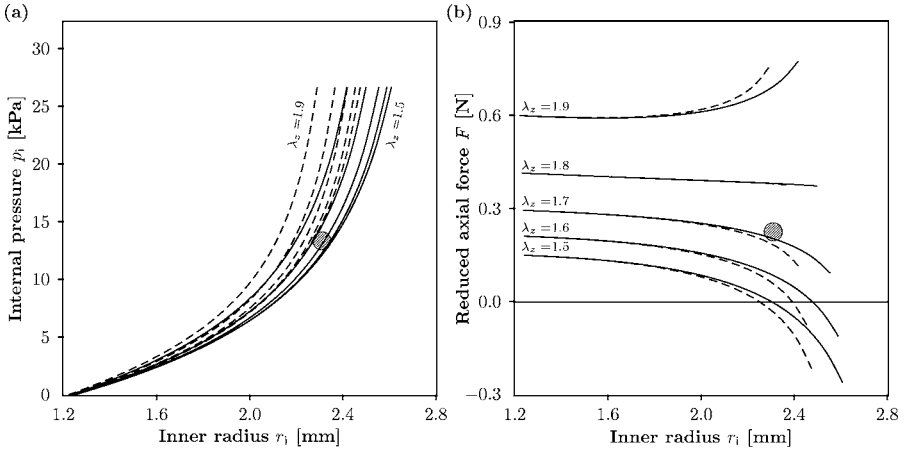

Figure 13. Deformation behavior of a dog carotid artery during inflation using the constitutive model in [59] (experiment D850815C). Solid lines are numerical results with residual strains included ($\alpha = 160.0°$) while the dashed lines are results without residual strains ($\alpha = 0.0°$). Dependence of (a) the internal pressure p_i and (b) the reduced axial force F on the inner radius r_i, without shear deformation ($\gamma_\mathrm{i} = 0$). The shaded circles indicate the approximate central region of the physiological state.

a dog carotid artery (see [59]) and the geometrical data used are summarized in Table V. We investigated the same range of loading as described in Section 4.2.3. The resulting arterial response is shown in Figure 13.

The potential (55) is able to represent the typical response of arteries quite well [59] except in the low pressure region, as also observed in Section 4.2.3 in respect of the potential (53). The residual stresses have a strong influence on the $p_\mathrm{i} - r_\mathrm{i}$ behavior. Finally, we remark that the potential (55), if used within a (displacement-driven) finite element formulation, may, because of the problems mentioned above, lead to numerical difficulties.

5. A Multi-Layer Model for Arterial Walls

In this section we propose a potential that models each layer of the artery as a fiber-reinforced composite. The basic idea is to formulate a constitutive model which incorporates some histological information. Hence, the material parameters involved may be associated with the histological structure of arterial walls (i.e. fiber directions), a feature which is not possible with the phenomenological models described so far in the paper. The underlying physical background of the proposed constitutive model leads to a formulation that avoids the problems encountered with some phenomenological models. The model is based on the theory of the mechanics of fiber-reinforced composites [57] and embodies the symmetries of a cylindrically orthotropic material.

5.1. CONSTITUTIVE MODEL FOR THE ARTERY LAYERS

Since arteries are composed of (thick-walled) layers we model each of these layers with a separate strain-energy function. From the engineering point of view each layer may be considered as a composite reinforced by two families of (collagen) fibers which are arranged in symmetrical spirals.

We assume that each layer responds with similar mechanical characteristics and we therefore use the same form of strain-energy function (but a different set of material parameters) for each layer. We suggest an additive split of the isochoric strain-energy function $\overline{\Psi}$ into a part $\overline{\Psi}_{\rm iso}$ associated with *iso*tropic deformations and a part $\overline{\Psi}_{\rm aniso}$ associated with *aniso*tropic deformations [29]. Since the (wavy) collagen fibers of arterial walls are not active at low pressures (they do not store strain energy) we associate $\overline{\Psi}_{\rm iso}$ with the mechanical response of the non-collagenous matrix material, which we assume to be isotropic. The resistance to stretch at high pressures is almost entirely due to collagenous fibers [49] and this mechanical response is therefore taken to be governed by the anisotropic function $\overline{\Psi}_{\rm aniso}$. Hence, the (two-term) potential is written as

$$\overline{\Psi}(\overline{\mathbf{C}}, \mathbf{a}_{0\,1}, \mathbf{a}_{0\,2}) = \overline{\Psi}_{\rm iso}(\overline{\mathbf{C}}) + \overline{\Psi}_{\rm aniso}(\overline{\mathbf{C}}, \mathbf{a}_{0\,1}, \mathbf{a}_{0\,2}), \tag{57}$$

where the families of collagenous fibers are characterized by the two (reference) direction vectors $\mathbf{a}_{0\,i}$, $i = 1, 2$, with $|\mathbf{a}_{0\,i}| = 1$. Note that in (57) we use $\overline{\mathbf{C}}$ rather than $\overline{\mathbf{E}}$ as the deformation measure.

We include structure tensors in accordance with the formulation in Section 3.1.2. Specifically, we incorporate two such tensors, $\mathbf{A}_i$, $i = 1, 2$, defined as the tensor products $\mathbf{a}_{0\,i} \otimes \mathbf{a}_{0\,i}$. The integrity basis for the three symmetric second-order tensors $\overline{\mathbf{C}}$, $\mathbf{A}_1$, $\mathbf{A}_2$ then consists of the invariants

$$\bar{I}_1(\overline{\mathbf{C}}) = \operatorname{tr} \overline{\mathbf{C}}, \qquad \bar{I}_2(\overline{\mathbf{C}}) = \frac{1}{2}[(\operatorname{tr} \overline{\mathbf{C}})^2 - \operatorname{tr} \overline{\mathbf{C}}^2], \qquad \bar{I}_3(\overline{\mathbf{C}}) = \det \overline{\mathbf{C}} = 1, \tag{58}$$

$$\bar{I}_4(\overline{\mathbf{C}}, \mathbf{a}_{0\,1}) = \overline{\mathbf{C}} : \mathbf{A}_1, \qquad \bar{I}_5(\overline{\mathbf{C}}, \mathbf{a}_{0\,1}) = \overline{\mathbf{C}}^2 : \mathbf{A}_1, \tag{59}$$

$$\bar{I}_6(\overline{\mathbf{C}}, \mathbf{a}_{02}) = \overline{\mathbf{C}} : \mathbf{A}_2, \qquad \bar{I}_7(\overline{\mathbf{C}}, \mathbf{a}_{02}) = \overline{\mathbf{C}}^2 : \mathbf{A}_2, \tag{60}$$

$$\bar{I}_8(\overline{\mathbf{C}}, \mathbf{a}_{01}, \mathbf{a}_{02}) = (\mathbf{a}_{01} \cdot \mathbf{a}_{02})\, \mathbf{a}_{01} \cdot \overline{\mathbf{C}}\mathbf{a}_{02}, \quad \bar{I}_9(\mathbf{a}_{01}, \mathbf{a}_{02}) = (\mathbf{a}_{01} \cdot \mathbf{a}_{02})^2; \tag{61}$$

see [57, 25]. Since the invariants $\bar{I}_3$, $\bar{I}_9$ are constants we may express equation (57) in the reduced form

$$\overline{\Psi}(\overline{\mathbf{C}}, \mathbf{A}_1, \mathbf{A}_2) = \overline{\Psi}_{\text{iso}}(\bar{I}_1, \bar{I}_2) + \overline{\Psi}_{\text{aniso}}(\bar{I}_1, \bar{I}_2, \bar{I}_4, \ldots, \bar{I}_8). \tag{62}$$

Note that the invariants $\bar{I}_4$ and $\bar{I}_6$ are the squares of the stretches in the directions of $\mathbf{a}_{01}$ and $\mathbf{a}_{02}$, respectively, so that they are stretch measures for the two families of (collagen) fibers and therefore have a clear physical interpretation. For simplicity, in order to minimize the number of material parameters, we consider the reduced form of (62) given by

$$\overline{\Psi}(\overline{\mathbf{C}}, \mathbf{A}_1, \mathbf{A}_2) = \overline{\Psi}_{\text{iso}}(\bar{I}_1) + \overline{\Psi}_{\text{aniso}}(\bar{I}_4, \bar{I}_6). \tag{63}$$

The anisotropy then arises only through the invariants $\bar{I}_4$ and $\bar{I}_6$, but this is sufficiently general to capture the typical features of arterial response.

Finally, the two contributions $\overline{\Psi}_{\text{iso}}$ and $\overline{\Psi}_{\text{aniso}}$ to the function $\overline{\Psi}$ must be particularized so as to fit the material parameters to the experimentally observed response of the arterial layers. We use the (classical) neo-Hookean model to determine the isotropic response in each layer, and we write

$$\overline{\Psi}_{\text{iso}}(\bar{I}_1) = \frac{c}{2}(\bar{I}_1 - 3), \tag{64}$$

where $c > 0$ is a stress-like material parameter. The strong stiffening effect of each layer observed at high pressures motivates the use of an exponential function for the description of the strain energy stored in the collagen fibers, and for this we propose

$$\overline{\Psi}_{\text{aniso}}(\bar{I}_4, \bar{I}_6) = \frac{k_1}{2k_2} \sum_{i=4,6} \left\{ \exp[k_2(\bar{I}_i - 1)^2] - 1 \right\}, \tag{65}$$

where $k_1 > 0$ is a stress-like material parameter and $k_2 > 0$ is a dimensionless parameter. An appropriate choice of k_1 and k_2 enables the histologically-based assumption that the collagen fibers do not influence the mechanical response of the artery in the low pressure domain [49] to be modeled.

All that remains is to determine an expression for the stress, which we provide here in the Eulerian description. Using $(10)_3$ and the proposed particularizations (64) and (65), we obtain, after some straightforward manipulations, the explicit isochoric contribution $\overline{\boldsymbol{\sigma}}$ to the Cauchy stress tensor, namely

$$\overline{\boldsymbol{\sigma}} = c\, \mathrm{dev}\, \overline{\mathbf{b}} + \sum_{i=4,6} 2\overline{\Psi}_i \mathrm{dev}(\mathbf{a}_i \otimes \mathbf{a}_i), \tag{66}$$

where $\overline{\Psi}_4 = \partial \overline{\Psi}_{\text{aniso}} / \partial \bar{I}_4$, $\overline{\Psi}_6 = \partial \overline{\Psi}_{\text{aniso}} / \partial \bar{I}_6$ denote (scalar) response functions and $\mathbf{a}_i = \overline{\mathbf{F}}\mathbf{a}_{0i}$, $i = 1, 2$, the Eulerian counterparts of $\mathbf{a}_{0i}$. For a detailed derivation

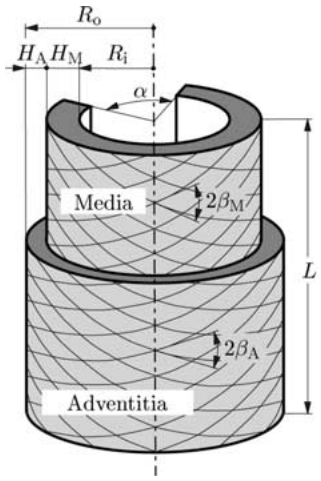

	Material	Geometry
Media	$c_M = 3.0000$ [kPa] $k_{1M} = 2.3632$ [kPa] $k_{2M} = 0.8393$ [–]	$H_M = 0.26$ [mm] $\beta_M = 29.0°$
Adventitia	$c_A = 0.3000$ [kPa] $k_{1A} = 0.5620$ [kPa] $k_{2A} = 0.7112$ [–]	$H_A = 0.13$ [mm] $\beta_A = 62.0°$

$R_i = 0.71$ [mm] for $\alpha = 0.0°$
$R_i = 1.43$ [mm] for $\alpha = 160.0°$

Figure 14. Material and geometrical data for a carotid artery from a rabbit in respect of (67) and (68) (see experiment 71 in [5]).

of equation (66) the reader is referred to the more general constitutive framework described in [20].

5.2. ARTERY MODELED AS A TWO-LAYER THICK-WALLED TUBE WITH RESIDUAL STRAINS

In order to report the performance of the proposed constitutive model we study the mechanical response of a *healthy young* arterial segment (with no pathological intimal changes). For this case the innermost layer of the artery is not of (solid) mechanical interest, and we therefore focus attention on modeling the two remaining layers, i.e. the media and the adventitia. It is then appropriate to model the artery as a two-layer thick-walled tube (with residual strains), as illustrated in Figure 14.

This model uses 6 material parameters, i.e. c_M, k_{1M}, k_{2M} for the media and c_A, k_{1A}, k_{2A} for the adventitia. In respect of equations (63)–(65) the free-energy functions for the considered two-layer problem may be written as

$$\overline{\Psi}_M = \frac{c_M}{2}(\bar{I}_1 - 3) + \frac{k_{1M}}{2k_{2M}} \sum_{i=4,6} \big\{\exp[k_{2M}(\bar{I}_{iM} - 1)^2] - 1\big\},$$
$$R_i \leqslant R \leqslant R_i + H_M, \tag{67}$$
$$\overline{\Psi}_A = \frac{c_A}{2}(\bar{I}_1 - 3) + \frac{k_{1A}}{2k_{2A}} \sum_{i=4,6} \big\{\exp[k_{2A}(\bar{I}_{iA} - 1)^2] - 1\big\},$$
$$R_i + H_M \leqslant R \leqslant R_o \tag{68}$$

for the media and adventitia, respectively. The constants c_M and c_A are associated with the non-collagenous matrix of the material, which describes the *isotropic* part of the overall response of the tissue. Note, however, that the matrix material is

significantly less stiff than its elastin fiber constituent. The constants $k_{1\,\mathrm{M}}$, $k_{2\,\mathrm{M}}$ and $k_{1\,\mathrm{A}}$, $k_{2\,\mathrm{A}}$ are associated with the *anisotropic* contribution of collagen to the overall response. The material parameters are constants and do not depend on the geometry, opening angle or fiber angle. The internal pressure/radius response, of course, does depend on geometry, opening angle and fiber angle, but we have not included here an analysis of the effect of changes in these quantities. However, our studies have found that in the high-pressure regime the stress–strain response depends significantly on the fiber angles (as should be expected). The fiber angles are associated with the stress-free configuration, as indicated in Figure 14, and we have assumed that they are the same in the load-free configuration. The difference in angle between the unstressed and unloaded configurations for the case we considered goes from (approximately) -3.0° on the inner boundary to $+2.7^\circ$ on the outer boundary (mean value 0.2°). This approximation has a negligible influence on the subsequent analysis.

The invariants, associated with the media M and the adventitia A, are defined by $\bar{I}_{4\,j} = \mathbf{A}_{1\,j} : \overline{\mathbf{C}}$ and $\bar{I}_{6\,j} = \mathbf{A}_{2\,j} : \overline{\mathbf{C}}$, $j = \mathrm{M}, \mathrm{A}$, and H_{M} is the reference thickness of the media, as illustrated in Figure 14. The tensors $\mathbf{A}_{1\,j}$, $\mathbf{A}_{2\,j}$, characterizing the structure of the media and adventitia, are given by

$$\mathbf{A}_{1\,j} = \mathbf{a}_{0\,1\,j} \otimes \mathbf{a}_{0\,1\,j}, \qquad \mathbf{A}_{2\,j} = \mathbf{a}_{0\,2\,j} \otimes \mathbf{a}_{0\,2\,j}, \quad j = \mathrm{M}, \mathrm{A}, \tag{69}$$

where, in a cylindrical polar coordinate system, the components of the direction vectors $\mathbf{a}_{0\,1\,j}$ and $\mathbf{a}_{0\,2\,j}$ have, in matrix notation, the forms

$$[\mathbf{a}_{0\,1\,j}] = \begin{bmatrix} 0 \\ \cos\beta_j \\ \sin\beta_j \end{bmatrix}, \qquad [\mathbf{a}_{0\,2\,j}] = \begin{bmatrix} 0 \\ \cos\beta_j \\ -\sin\beta_j \end{bmatrix}, \quad j = \mathrm{M}, \mathrm{A}, \tag{70}$$

and β_j, $j = \mathrm{M}, A$, are the angles between the collagen fibers (arranged in symmetrical spirals) and the circumferential direction in the media and adventitia, as indicated in Figure 14. Note that Finlay et al. [13] reported that in, for example, human brain arteries the (collagenous) fiber orientations also have small components in the radial direction. However, we neglect this feature in the present work.

Because of the wavy structure of collagen it is regarded as not being able to support compressive stresses. We therefore assume that the fibers are active in extension and inactive in compression. Hence, in the proposed model the anisotropic terms in the free-energy functions (67) and (68) should only contribute when the fibers are extended, that is when $\bar{I}_{4\,j} > 1$ or $\bar{I}_{6\,j} > 1$, $j = \mathrm{M}, \mathrm{A}$. If one or more of these conditions is not satisfied then the relevant part of the anisotropic function is omitted from the expressions (67) and (68). If, for example, $\bar{I}_{4\,\mathrm{A}}$ and $\bar{I}_{6\,\mathrm{A}}$ are less than or equal to 1, then the response of the adventitia is purely isotropic. When these conditions are taken into account, convexity is guaranteed by the form of the free-energy functions (67) and (68).

Contour plots for the two arterial layers (media and adventitia) based on the material parameters given in Figure 14 are depicted in Figure 15. As can be seen,

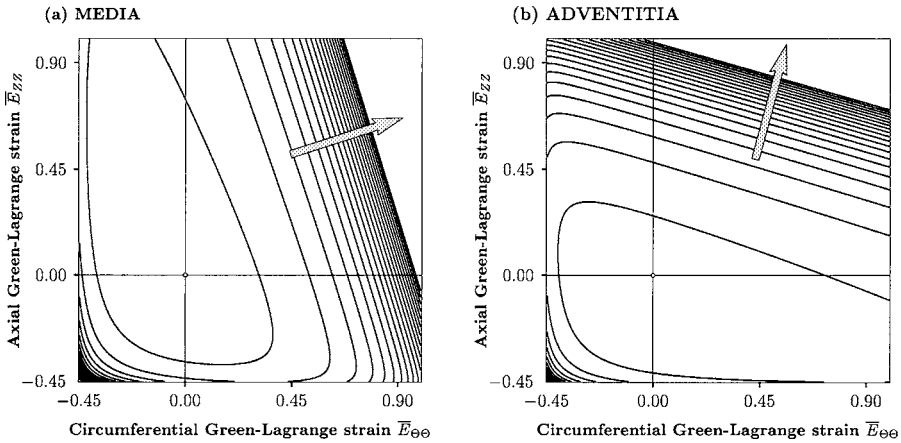

Figure 15. Contour plots of the potentials (67) for the media (a) and (68) for the adventitia (b) using material parameters given in Figure 14. The arrows show the directions of greatest ascent in the regions $\overline{E}_{\Theta\Theta} \geqslant 0$, $\overline{E}_{ZZ} \geqslant 0$.

the two potentials are convex and anisotropic. In addition, the directions of greatest ascent (illustrated by arrows in Figure 15) in the region $\overline{E}_{\Theta\Theta} \geqslant 0$, $\overline{E}_{ZZ} \geqslant 0$ are clearly different for the two layers. These directions are determined mainly by the orientations of the collagen fibers, which tend to be nearly circumferential in the media and nearly axial in the adventitia. Note that where $\overline{E}_{\Theta\Theta} < 0$ and $\overline{E}_{ZZ} < 0$ the (symmetric) contours reflect the isotropy in this region.

Experimental tests performed by Von Maltzahn et al. [39], Yu et al. [69] and Xie et al. [68] indicate that the elastic properties of the media and adventitia are different. Their results show that the media is much stiffer than the adventitia. In particular, it was found that in the neighborhood of the reference configuration the mean value of Young's modulus for the media, for several pig thoracic aortas, is about an *order of magnitude higher* than that of the adventitia [69]. For our proposed constitutive model this observation implies that for these materials the neo-Hookean parameters are such that the ratio $c_{\mathrm{M}}/c_{\mathrm{A}}$ is typically in the range of 6 to 14. This effectively reduces the number of material parameters, and for definiteness we therefore set $c_{\mathrm{M}} = 10c_{\mathrm{A}}$ for purposes of numerical calculation. In general, however, this ratio depends on the topographical site.

We use geometrical data from [5] for a carotid artery from a rabbit (experiment 71 in [18]) and make the assumptions that the media occupies $2/3$ of the arterial wall thickness and that the wall thickness of each layer in the unloaded configuration ($\alpha = 0.0°$) is the same as for the case without residual stress ($\alpha = 160.0°$). In order to identify the material parameters of the two-layer model for healthy arterial walls, we fitted the parameters to the experimental data from experiment 71 in [18] and used the standard nonlinear *Levenberg–Marquardt* algorithm. The material parameters obtained are summarized in Figure 14. For more explanation of the underlying fitting process the reader is referred to [21]. For purposes of

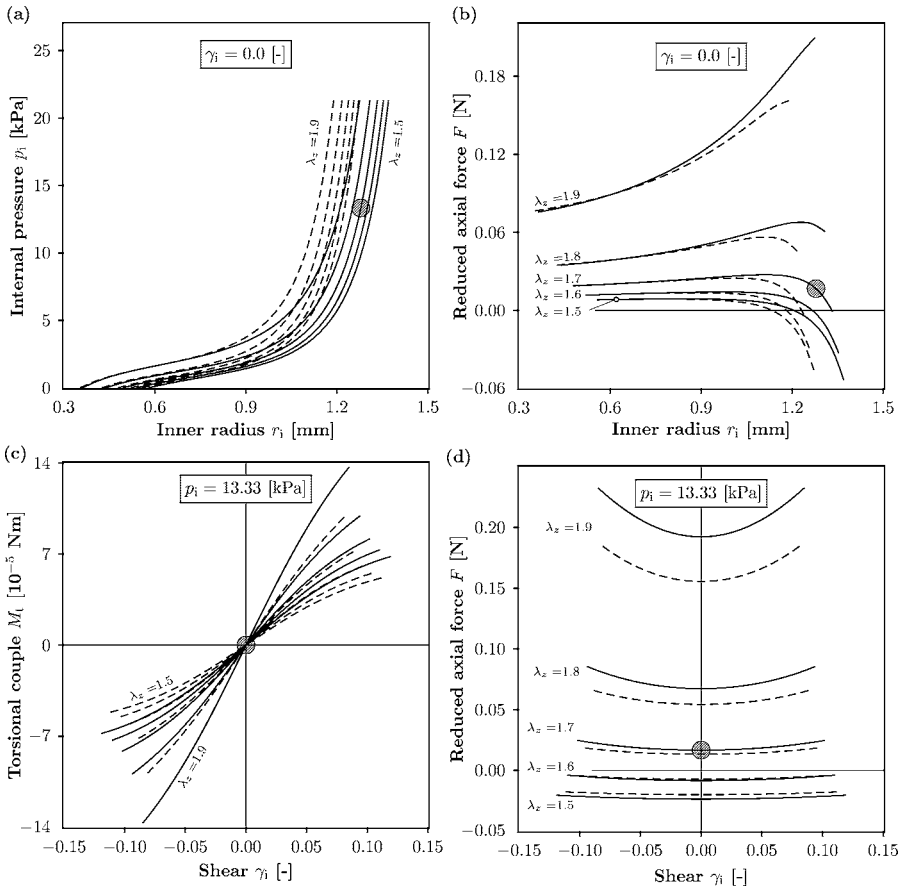

Figure 16. Deformation behavior of a carotid artery during inflation and torsion using the constitutive model (67)–(68). Solid lines are numerical results with residual strains included ($\alpha = 160.0°$) and the dashed lines are results without residual strains ($\alpha = 0.0°$). Dependence of (a) the internal pressure p_i and (b) the reduced axial force F on inner radius r_i, without shear deformation ($\gamma_i = 0$). Dependence of (c) the torsional couple M_t and (d) the reduced axial force F on the shear γ_i at fixed internal pressure $p_i = 13.33$ [kPa]. The shaded circles indicate the approximate central region of the physiological state.

comparison, we make the assumption that the configuration shown in Figure 14 is stress-free. But, bearing in mind the discussion in Section 3.2.1 concerning a single layer, this simplifying assumption must be regarded as an approximation. In practice, the opening angles and the stress-free configurations for the separate layers would be different.

The mechanical response of the carotid artery during bending, inflation, axial extension and torsion is shown in Figure 16. The internal pressure p_i and the angle of twist Φ are varied within the ranges

$$0 \leqslant p_i \leqslant 21.33 \text{ [kPa]} \quad \text{and} \quad -0.10 \leqslant \Phi \leqslant 0.10 \text{ [rad]}. \tag{71}$$

The internal pressure versus radius behavior in the low pressure domain shown in Figure 16(a) clearly differs from the pressure/radius curves discussed in previous sections, as comparison with Figures 5(a), 7(a), 9(a), 11(a) and 13(a) shows. The proposed model (67)–(68) is able to describe the salient features of arterial elasticity, such as the experimentally observed 'sigma-shaped' form of the pressure/radius relationship; see Figure 2(a) in [66]. Note that residual strains have a strong influence on the global pressure/radius response of the artery, which is similar to what was observed for the other potentials treated in this paper except for that in [10], as discussed in Section 4.1.1, for which $\alpha = 100.0^\circ$ and a smaller value of the wall thickness to diameter ratio was used.

Figure 16(b) shows that the proposed potential (67)–(68) is also able to model the typical evolution of the reduced axial force F with inflation (increase of the inner radius) of the artery; see Figure 2(b) in [66]. This means that F is a decreasing function of r_{i} at axial stretches λ_z less than some value above the physiological stretch and an increasing function for λ_z greater than this value (this effect is also evident in Figure 7(b)). This characteristic behavior can also be replicated with the other potentials described in Section 4 except for the constitutive model in [62]; see Figure 9(b).

The response of the artery during torsion at the internal (physiological) pressure $p_{\mathrm{i}} = 13.33$ [kPa] is plotted in Figure 16(c), (d). As can be seen from Figure 16(c), the torsional couple M_{t} increases more slowly than the shear $\gamma_{\mathrm{i}} = \Phi r_{\mathrm{i}}/l = \Phi r_{\mathrm{i}}/\lambda_z L$ on the inner boundary increases (i.e. the slope of the curve decreases). One possible explanation of this interesting phenomenon is as follows: since the artery is inflated with the internal physiological pressure, the (collagen) fiber reinforcement is activated and the fibers are much stiffer than the matrix material. During torsion from this state of deformation the nearly inextensible fibers cause the arterial diameter to decrease, which leads to a reduction in the torsional couple M_{t} given by equation $(26)_2$. This realistic diameter-shrinking behavior of the artery during torsion seems to be a consequence of the considered fiber reinforcement (orthotropy). However, this effect may also be predicted by a non-convex isotropic strain-energy function. Of the potentials discussed in Section 4 only that reviewed in Section 4.1.2 can predict this phenomenon (see Figure 7(c)).

In Figure 16(d) the reduced axial force F during torsion is plotted against the shear γ_{i}. For an axial pre-stretch $\lambda_z = 1.5$ the reduction in the inner radius r_{i} due to torsion is about 5.8% ($\gamma_{\mathrm{i}} = 0.119$) and 7.8% for $\lambda_z = 1.9$ ($\gamma_{\mathrm{i}} = 0.085$). This behavior is in qualitative agreement with experimental observations presented in [12] and may also be reproduced with the potentials described in Sections 4.1.1 and 4.1.2; see Figures 5(d), 7(d). Note the relatively strong influence of residual strains at high axial stretches compared with that shown in Figure 7(d).

REMARK 5.1. The fully three-dimensional formulation of the convex potential (67)–(68) allows the characteristic anisotropic behavior of healthy arteries under combined bending, inflation, axial extension and torsion to be predicted. It is not, however, restricted to a particular geometry such as axisymmetry, and is

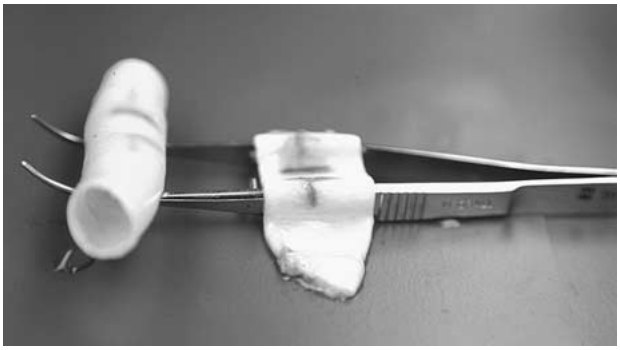

Figure 17. Mechanical separation of the layers of a human external iliac artery into a stiff media-intima tube (on the left-hand side) and a limp adventitia (from *C. Schulze-Bauer, MD*, Computational Biomechanics, Graz University of Technology, Austria, with permission).

accessible to approximation techniques such as the finite element method. For an extension of the anisotropic model to the finite viscoelastic domain see [26] and for an extension of the constitutive framework to the elastoplastic domain see [20] and [21]. All these recent works focus on implementation of the models in a finite element program.

The proposed constitutive model has the merit that it is based partly on histological information. It therefore allows the material parameters to be associated with the constituents (matrix and collagen) of each solid mechanically-relevant layer. Since the media and adventitia have different physiological functions, a two-layer model using different strain-energy functions for the media and adventitia seems to be essential. This idea goes back to von Maltzahn et al. [38], who proposed a cylindrical two-layer model using an isotropic (polynomial) function (with one coefficient) for the media and an anisotropic strain-energy function for the adventitia (with three coefficients). This approach is indispensable for the study of stress distributions across the arterial wall and allows a histomechanical investigation of the arterial layers and their underlying physiological functions. Extension to a three-layer constitutive model incorporating pathological intimal changes is a straightforward task.

Figure 17, in which mechanically separated media-intima and adventitia layers are shown, provides a graphic illustration of the effect of the different properties and (possibly) different residual stresses in the two tubes. In the unloaded configuration the relevant geometrical quantities are – media-intima: inner radius, 4.07 [mm]; thickness 0.98 [mm]; adventitia: thickness 0.4 [mm]. The given geometry should be taken into account in interpreting the figure.

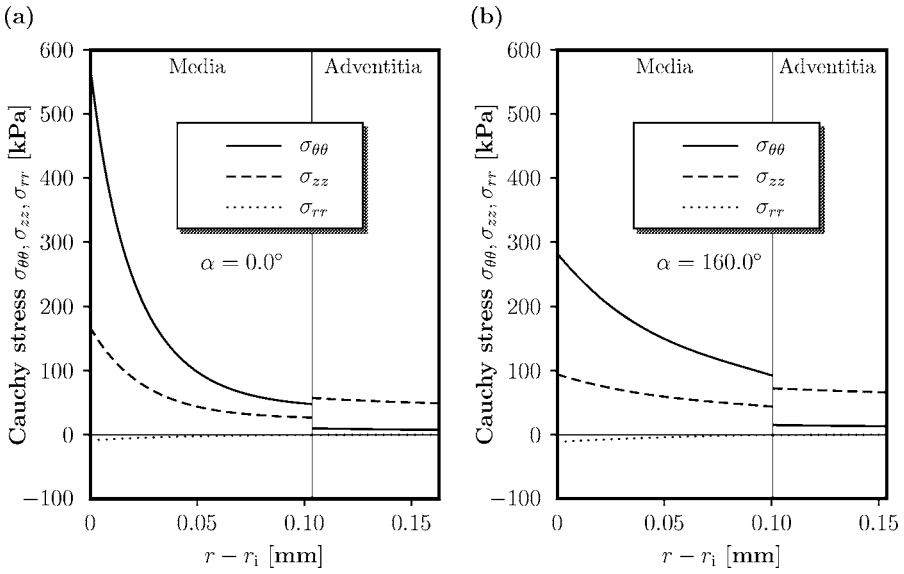

Figure 18. Plots of the principal Cauchy stresses $\sigma_{\theta\theta}$, σ_{zz}, σ_{rr} in the circumferential, axial and radial directions through the deformed media and adventitia layers in the physiological state with $p_i = 13.33$ [kPa], $\lambda_z = 1.7$, $\gamma_i = 0$: (a) without residual stress ($\alpha = 0.0°$); (b) with residual stress ($\alpha = 160.0°$). The abscissa is $r - r_i$. The numerical results are obtained for the constitutive models (67) and (68) with geometrical data and material constants as in Figure 14.

5.3. STRESS DISTRIBUTION THROUGH THE DEFORMED ARTERIAL WALL

One important aspect of the influence of residual stress is the effect that it has on the stress distribution through the arterial wall in the physiological state. Whilst we have seen from, for example, Figure 16 its effect on the overall pressure/radius response its effect on the stress distribution through the arterial wall is more pronounced. This is illustrated in Figure 18, in which the distributions of the principal Cauchy stress components $\sigma_{\theta\theta}$, σ_{zz} and σ_{rr} through the deformed wall thickness (media and adventitia layers) are plotted against $r - r_i$, where r is the deformed radial coordinate and r_i the deformed inner radius. The geometrical data and material constants shown in Figure 14 are again used in conjunction with the material models (67) and (68). The physiological state is taken to correspond to $p_i = 13.33$ [kPa] and $\lambda_z = 1.7$, with no torsion ($\gamma_i = 0$). The calculation can be carried out by using any numerical tool. However, in order to solve the three-dimensional boundary-value problem for the stress components $\sigma_{\theta\theta}$, σ_{zz} and σ_{rr} (rather than for $\overline{\sigma}_{\theta\theta}$, $\overline{\sigma}_{zz}$ and $\overline{\sigma}_{rr}$, as used throughout the text) it seems to be convenient to employ the (mixed) finite element method. Details of the computational aspects are described in Holzapfel and Gasser [26].

Figure 18(a) shows the Cauchy stress distributions for the case in which there are no residual stresses ($\alpha = 0.0°$), while Figure 18(b) shows the corresponding plot with residual stresses included ($\alpha = 160.0°$). The tangential stresses $\sigma_{\theta\theta}$ and

σ_{zz} are discontinous at the media/adventitia interface, while the radial stress σ_{rr} is continuous. Note that the magnitude of σ_{rr} is much smaller than that of the tangential stresses. The behavior shown in Figure 18(a) is similar to that found by Von Maltzahn and Warriyar [39] for bovine carotid arteries. Figure 18 demonstrates the relatively high values of the circumferential stress in the media compared with that in the adventitia, which was also found, for example, in [39]. Within the media there is a significant difference between the distributions of $\sigma_{\theta\theta}$ and σ_{zz} in the two plots. Interestingly, although the maximum circumferential stress $\sigma_{\theta\theta}$ (which occurs at the inner wall) is reduced significantly, the mean circumferential stress through the wall is increased by the presence of residual stress. Note that the residual stress also influences the deformed wall thickness and the strains in the physiological state. In particular, at the inner wall, for example, the circumferential strain (measured relative to the stress-free configuration) is reduced by the residual stress.

The most important influence of the residual stress is the reduction in the maximum stress values $\sigma_{\theta\theta}$ and σ_{zz} (which occur at the inner side of the media) and the gradients of $\sigma_{\theta\theta}$ and σ_{zz} in the media, an effect which has been reported previously for a single layer (see, for example, Fung [16], Section 11.3). Stress gradients would be reduced further by larger values of α, as has also been described in [16]. Indeed, it is often assumed that the arterial wall adapts itself so that the circumferential stresses are uniform within each layer. Moreover, the assumption of uniform strain is sometimes adopted (see, for example, Takamizawa and Hayashi [59]). Some consequences of these assumptions have been discussed in a recent paper by Ogden and Schulze-Bauer [43].

6. Summary and Concluding Remarks

For a deeper understanding of the highly nonlinear deformation mechanisms and stress distributions in arteries under different loading conditions and the improvement of diagnostics and therapeutical procedures that are based on mechanical treatments, a reliable constitutive model of arteries is an essential prerequisite.

For the description of the nonlinear elastic behavior of arterial walls, there are essentially polynomial, exponential and logarithmic forms of strain-energy function available in the literature. A representative selection of models in common use has been investigated in this paper and evaluated in detail. This comparative study was conducted in respect of the mechanical response of a thick-walled tube under combined bending, inflation, axial extension and torsion and with reference to fundamental continuum mechanical principles. It is hoped that this simple study will offer some guidance for the evaluation of alternative forms of strain-energy function for arteries.

The constitutive model of Delfino et al. [10], which is based on an isotropic description, is not able to reproduce the pronounced anisotropic mechanical behavior of arteries observed in several experimental investigations. Nevertheless, it is worth

noting that its predictions for the restricted kinematics and loading conditions considered here are in some respects qualitatively similar to those for the anisotropic energy functions discussed in Section 4.

The two-dimensional formulation discussed in Section 4.2.1 does not, in general, permit the stress response under certain combined loadings (such as inflation and torsion) to be modeled. Exceptionally, if the material is isotropic or if it describes a membrane model, such combined loadings can be analyzed, as shown in Section 4.2.1. However, such a formulation, because it omits $\overline{E}_{R\Theta}$, $\overline{E}_{RZ}$ and $\overline{E}_{RR}$, is inherently limited to specific kinematics or to a membrane description. For example, if $\overline{E}_{RR}$ is omitted then the inflation/torsion problem cannot be solved for a thick-walled tube. The three well-established anisotropic models developed by Vaishnav et al. [62], Fung et al. [18] and Takamizawa and Hayashi [59], which we have discussed in Section 4.2, are special cases of this two-dimensional formulation. *A fortiori*, their applicability is limited, but, as we have seen, they do predict qualitatively reasonable response for restricted geometry and loadings. Moreover, they have contributed to our current level of understanding of arterial wall mechanics. Thus, isotropic or two-dimensional anisotropic energy functions may be valuable under some conditions, but, bearing in mind the limitations discussed above, they should be used with caution.

In the theory of elasticity the notion of convexity of the strain-energy function (which is dependent on the choice of deformation measure used) has an important role in ensuring physically meaningful and unambiguous mechanical behavior. It also induces desirable mathematical features in the governing equations, which are important from the point of view of numerical computations. A problem detected in the potentials considered in this comparative study is the general lack of convexity. For example, the anisotropic potential of Vaishnav et al. [62] is not convex for *any* set of material parameters. The strain-energy functions of Fung et al. [18], Chuong and Fung [5] and Takamizawa and Hayashi [59] are not convex for all possible sets of material parameters, and restrictions on these parameters are therefore needed to ensure convexity and, therefore, to avoid material instabilities.

The three-dimensional anisotropic mechanical response of arteries points to the need for three-dimensional constitutive models, and suitable generalizations of the above-mentioned models must therefore be employed. All the models discussed above are based on a phenomenological approach in which the *macroscopic* nature of the biological material is modeled. This approach, which is concerned mainly with fitting the constitutive equations to experimental data, is not capable of relating the deformation mechanism to the known architectural structure of the arterial wall. The material parameters have no direct physical meaning and are therefore treated as numbers without clear physical interpretation.

From this comparative study and the experience gained, it may be concluded that there is a need for an alternative form of constitutive model which avoids the limitations discussed. It is for this reason that we have proposed an approach in which arterial walls are approximated as two-layer thick-walled tubes, with each

layer modeled as a highly deformable fiber-reinforced composite. This leads to a fully three-dimensional anisotropic material description of the artery incorporating histological information. The proposed two-layer model uses a set of *six* material parameters whose interpretations can be partly based on the underlying histological structure.

The new model discussed in this paper is consistent with both mechanical and mathematical requirements and is suitable for use within the context of finite element methods (see, for example, [26, 20] and [21]). It is also applicable for arbitrary geometries so that more complex boundary-value problems can be solved. As described in Section 5.3, this approach enables insight into the nature of the stress distribution across the arterial wall to be gained, and therefore offers the potential for a detailed study of the mechanical functionality of arteries.

The importance of including residual strains (and stresses), which was shown previously by scientists such as Chuong and Fung [6], has been emphasized. As we have seen, incorporation of residual strains in the load-free configuration changes not only the overall pressure/radius response of the artery but also the stress distribution through the deformed arterial wall (see also [5]). Thus, in order to predict reliable stress distributions, the parameter identification process must incorporate residual strains in the load-free configuration.

Acknowledgements

Financial support for this research was provided by the *Austrian Science Foundation* under *START-Award Y74-TEC* and *FWF-Project No. P11899-TEC*. This support is gratefully acknowledged. Ray Ogden is grateful to Graz University of Technology for support during several visits and to the British Council in Vienna for financial support for this research. The authors are indebted to *C.A.J. Schulze-Bauer, MD* for his contributions to this work and for valuable discussions.

References

1. H. Abè, K. Hayashi and M. Sato (eds), *Data Book on Mechanical Properties of Living Cells, Tissues, and Organs*, Springer-Verlag, New York (1996).
2. H. Bader, Dependence of wall stress in the human thoracic aorta on age and pressure. *Circ. Res.* **20** (1967) 354–361.
3. P.C. Block, Mechanism of transluminal angioplasty. *Am. J. Cardiology* **53** (1984) 69C–71C.
4. T.E. Carew, R.N. Vaishnav and D.J. Patel, Compressibility of the arterial wall. *Circ. Res.* **23** (1968) 61–68.
5. C.J. Chuong and Y.C. Fung, Three-dimensional stress distribution in arteries. *J. Biomech. Engr.* **105** (1983) 268–274.
6. C.J. Chuong and Y.C. Fung, Residual stress in arteries. In: G.W. Schmid-Schönbein, S.L-Y. Woo and B.W. Zweifach (eds), *Frontiers in Biomechanics*, Springer-Verlag, New York (1986), pp. 117–129.
7. P.G. Ciarlet, *Mathematical Elasticity. Volume I: Three-Dimensional Elasticity*, North-Holland, Amsterdam (1988).

8. R.H. Cox, Regional variation of series elasticity in canine arterial smooth muscles. *Am. J. Physiol.* **234** (1978) H542–H551.
9. R.H. Cox, Comparison of arterial wall mechanics using ring and cylindrical segments. *Am. J. Phys.* **244** (1983) H298–H303.
10. A. Delfino, N. Stergiopulos, J.E. Moore and J.-J. Meister, Residual strain effects on the stress field in a thick wall finite element model of the human carotid bifurcation. *J. Biomech.* **30** (1997) 777–786.
11. H. Demiray, A layered cylindrical shell model for an aorta. *Int. J. Engr. Sci.* **29** (1991) 47–54.
12. S.X. Deng, J. Tomioka, J.C. Debes and Y.C. Fung, New experiments on shear modulus of elasticity of arteries. *Am. J. Physiol.* **266** (1994) H1–H10.
13. H.M. Finlay, L. McCullough and P.B. Canham, Three-dimensional collagen organization of human brain arteries at different transmural pressures. *J. Vasc. Res.* **32** (1995) 301–312.
14. P. Flory, Thermodynamic relations for high elastic materials. *Trans. Faraday Soc.* **57** (1961) 829–838.
15. R.F. Fuchs, Zur Physiologie und Wachstumsmechanik des Blutgefäßsystems. *Archiv für die gesamte Physiologie* **28** (1900).
16. Y.C. Fung, *Biomechanics: Motion, Flow, Stress, and Growth*, Springer-Verlag, New York (1990).
17. Y.C. Fung, *Biomechanics: Mechanical Properties of Living Tissue*, 2nd edn, Springer-Verlag, New York (1993).
18. Y.C. Fung, K. Fronek and P. Patitucci, Pseudoelasticity of arteries and the choice of its mathematical expression. *Am. J. Physiol.* **237** (1979) H620–H631.
19. Y.C. Fung and S.Q. Liu, Change of residual strains in arteries due to hypertrophy caused by aortic constriction. *Circ. Res.* **65** (1989) 1340–1349.
20. T.C. Gasser and G.A. Holzapfel, Rate-independent elastoplastic constitutive modeling of biological soft tissues: Part I. Continuum basis, algorithmic formulation and finite element implementation. Submitted (2000).
21. T.C. Gasser, C.A.J. Schulze-Bauer, E. Pernkopf, M. Stadler and G.A. Holzapfel, Rate-independent elastoplastic constitutive modeling of biological soft tissues: Part II. Percutaneous transluminal angioplasty. Submitted (2000).
22. J.M. Guccione, A.D. McCulloch and L.K. Waldman, Passive material properties of intact ventricular myocardium determined from a cylindrical model. *ASME J. Biomech. Engr.* **113** (1991) 42–55.
23. H.C. Han and Y.C. Fung, Species dependence of the zero-stress state of aorta: Pig versus rat. *J. Biomech. Engr.* **113** (1991) 446–451.
24. K. Hayashi, Experimental approaches on measuring the mechanical properties and constitutive laws of arterial walls. *J. Biomech. Engr.* **115** (1993) 481–488.
25. G.A. Holzapfel, *Nonlinear Solid Mechanics. A Continuum Approach for Engineering*, Wiley, Chichester (2000).
26. G.A. Holzapfel and T.C. Gasser, A viscoelastic model for fiber-reinforced composites at finite strains: Continuum basis, computational aspects and applications. *Comput. Methods Appl. Mech. Engr.* In press (2000).
27. G.A. Holzapfel, T.C. Gasser, M. Stadler and C.A.J. Schulze-Bauer, A multi-layer structural model for the elastic and viscoelastic behavior of arterial walls: Continuum formulation and finite element analysis. Submitted (2000).
28. G.A. Holzapfel, C.A.J. Schulze-Bauer and M. Stadler, Mechanics of angioplasty: Wall, balloon and stent. In: J. Casey and G. Bao (eds), *Mechanics in Biology*, AMD-Vol. 242/BED-Vol. 46, The American Society of Mechanical Engineers, New York (2000), pp. 141–156.
29. G.A. Holzapfel and H.W. Weizsäcker, Biomechanical behavior of the arterial wall and its numerical characterization. *Comp. Biol. Med.* **28** (1998) 377–392.

30. W.H. Hoppmann and L. Wan, Large deformation of elastic tubes. *J. Biomech.* **3** (1970) 593–600.
31. T.J.R. Hughes, *The Finite Element Method: Linear Static and Dynamic Finite Element Analysis*, Prentice-Hall, Englewood Cliffs, NJ (1987).
32. J.D. Humphrey, Mechanics of arterial wall: Review and directions. *Critical Reviews in Biomed. Engr.* **23** (1995) 1–162.
33. J.D. Humphrey, An evaluation of pseudoelastic descriptors used in arterial mechanics. *J. Biomech. Engr.* **121** (1999) 259–262.
34. J.M. Huyghe, D.H. van Campen, T. Arts and R.M. Heethaar, A two-phase finite element model of the diastolic left ventricle. *J. Biomech.* **24** (1991) 527–538.
35. V.A. Kas'yanov and A.I. Rachev, Deformation of blood vessels upon stretching, internal pressure, and torsion. *Mech. Comp. Mat.* **16** (1980) 76–80.
36. Y. Lanir and Y.C. Fung, Two-dimensional mechanical properties of rabbit skin-I. Experimental system. *J. Biomech.* **7** (1974) 29–34.
37. B.M. Learoyd and M.G. Taylor, Alterations with age in the viscoelastic properties of human arterial walls. *Circ. Res.* **18** (1966) 278–292.
38. W.-W. Von Maltzahn, D. Besdo and W. Wiemer, Elastic properties of arteries: A nonlinear two-layer cylindrical model. *J. Biomech.* **14** (1981) 389–397.
39. W.-W. Von Maltzahn and R.G. Warriyar, Experimental measurments of elastic properties of media and adventitia of bovine carotid arteries. *J. Biomech.* **17** (1984) 839–847.
40. W.W. Nichols and M.F. O'Rourke, *McDonald's Blood Flow in Arteries*, 4th edn, Arnold, London (1998), chapter 4, pp. 73–97.
41. R.W. Ogden, Nearly isochoric elastic deformations: Application to rubberlike solids. *J. Mech. Phys. Solids* **26** (1978) 37–57.
42. R.W. Ogden, *Non-linear Elastic Deformations*, Dover Publication, New York (1997).
43. R.W. Ogden and C.A.J. Schulze-Bauer, Phenomenological and structural aspects of the mechanical response of arteries. In: J. Casey and G. Bao (eds), *Mechanics in Biology*, AMD-Vol. 242/BED-Vol. 46, The American Society of Mechanical Engineers, New York (2000), pp. 125–140.
44. H.S. Oktay, T. Kang, J. D. Humphrey and G.G. Bishop, Changes in the mechanical behavior of arteries following balloon angioplasty. In: *1991 ASME Advances in Bioengineering*, New York (1991).
45. D.J. Patel and D.L. Fry, The elastic symmetry of arterial segments in dogs. *Circ. Res.* **24** (1969) 1–8.
46. A. Rachev, Theoretical study of the effect of stress-dependent remodeling on arterial geometry under hypertensive conditions. *J. Biomech.* **30** (1997) 819–827.
47. A. Rachev and K. Hayashi, Theoretical study of the effects of vascular smooth muscle contraction on strain and stress distributions in arteries. *Ann. Biomed. Engr.* **27** (1999) 459–468.
48. J.A.G. Rhodin, Architecture of the vessel wall. In: H.V. Sparks Jr., D.F. Bohr, A.D. Somlyo and S.R. Geiger (eds), *Handbook of Physiology, The Cardiovascular System*, Vol. 2, American Physiologial Society, Bethesda, Maryland (1980), pp. 1–31.
49. M.R. Roach and A.C. Burton, The reason for the shape of the distensibility curve of arteries. *Canad. J. Biochem. Physiol.* **35** (1957) 681–690.
50. E.K. Rodriguez, A. Hoger and A.D. McCulloch, Stress-dependent finite growth in soft elastic tissues. *J. Biomech.* **27** (1994) 455–467.
51. C.S. Roy, The elastic properties of the arterial wall. *J. Physiol.* **3** (1880–1882) 125–159.
52. B.S. Schultze-Jena, Über die schraubenförmige Struktur der Arterienwand. *Gegenbauers Morphol. Jahrbuch* **83** (1939) 230–246.
53. C.A.J. Schulze-Bauer, C. Mörth and G.A. Holzapfel, Passive biaxial mechanical response of aged human iliac arteries. Submitted (2000).

54. F.H. Silver, D.L. Christiansen and C.M. Buntin, Mechanical properties of the aorta: A review. *Critical Reviews in Biomed. Engr.* **17** (1989) 323–358.
55. B.R. Simon, M.V. Kaufmann, M.A. McAfee and A.L. Baldwin, Porohyperelastic finite element analysis of large arteries using ABAQUS. *J. Biomech. Engr.* **120** (1998) 296–298.
56. B.R. Simon, M.V. Kaufmann, M.A. McAfee, A.L. Baldwin and L.M. Wilson, Identification and determination of material properties for porohyperelastic analysis of large arteries. *J. Biomech. Engr.* **120** (1998) 188–194.
57. A.J.M. Spencer, Constitutive theory for strongly anisotropic solids, In: A.J.M. Spencer (ed.), *Continuum Theory of the Mechanics of Fibre-Reinforced Composites*, CISM Courses and Lectures No. 282, International Centre for Mechanical Sciences, Springer-Verlag, Wien (1984), pp. 1–32.
58. J. Staubesand, Anatomie der Blutgefäße. I. Funktionelle Morphologie der Arterien, Venen und arterio-venösen Anastomosen. In: M. Ratschow (ed.), *Angiology*, Thieme, Stuttgart (1959), Chapter 2, pp. 23–82.
59. K. Takamizawa and K. Hayashi, Strain energy density function and uniform strain hypothesis for arterial mechanics. *J. Biomech.* **20** (1987) 7–17.
60. A. Tözeren, Elastic properties of arteries and their influence on the cardiovascular system. *J. Biomech. Engr.* **106** (1984) 182–185.
61. R.N. Vaishnav and J. Vossoughi, Estimation of residual strains in aortic segments. In: C.W. Hall (ed.), *Biomedical Engineering II: Recent Developments*, Pergamon Press, New York (1983), pp. 330–333.
62. R.N. Vaishnav, J.T. Young and D.J. Patel, Distribution of stresses and of strain-energy density through the wall thickness in a canine aortic segment. *Circ. Res.* **32** (1973) 577–583.
63. D.A. Vorp, K.R. Rajagopal, P.J. Smolinsky and H.S. Borovetz, Identification of elastic properties of homogeneous orthotropic vascular segments in distension. *J. Biomech.* **28** (1995) 501–512.
64. J. Vossoughi, Z. Hedjazi and F.S.I. Boriss, Intimal residual stress and strain in large arteries. In: *1993 ASME Advances in Bioengineering*, New York (1993), pp. 434–437.
65. J. Vossoughi and A. Tözeren, Determination of an effective shear modulus of aorta. *Russian J. Biomech.* **1**–**2** (1998) 20–35.
66. H.W. Weizsäcker and J.G. Pinto, Isotropy and anisotropy of the arterial wall. *J. Biomech.* **21** (1988) 477–487.
67. F.L. Wuyts, V.J. Vanhuyse, G.J. Langewouters, W.F. Decraemer, E.R. Raman and S. Buyle, Elastic properties of human aortas in relation to age and atherosclerosis: A structural model. *Phys. Med. Biol.* **40** (1995) 1577–1597.
68. J. Xie, J. Zhou and Y.C. Fung, Bending of blood vessel wall: Stress–strain laws of the intima-media and adventitia layers. *J. Biomech. Engr.* **117** (1995) 136–145.
69. Q. Yu, J. Zhou and Y.C. Fung, Neutral axis location in bending and Young's modulus of different layers of arterial wall. *Am. J. Physiol.* **265** (1993) H52–H60.